**Evaluation of the influence of the speed, preload and span length on the contact forces in the interaction between the pantograph and the overhead conductor rail.**

Montserrat Simarro[a], Juan Jesús Castillo[a], Juan A. Cabrera[a], Sergio Postigo[a]*

a. Department of Mechanical Engineering, Thermal and Fluid Mechanics, University of Malaga, Spain.

E-mail addresses: msimarro@uma.es (M. Simarro), juancas@uma.es (J.J. Castillo), jcabrera@uma.es (J. Cabrera), spostigo@uma.es (S. Postigo).

* Corresponding author:

Sergio Postigo Pozo

Departamento de Ingeniería Mecánica, Térmica y de Fluidos [Department of Mechanical Engineering, Thermal and Fluid Mechanics]

Universidad de Málaga [University of Malaga]

Escuela de Ingenierías [School of Engineering]

C/ Doctor Ortiz Ramos S/N

Campus de Teatinos

29071 Málaga (Spain)

Phone: +34 951952534

Email: spostigo@uma.es

## Conflict of interest statement

The authors have no financial or personal relationships that could inappropriately influence the work reported in this manuscript.

**Keywords**
Contact forces, overhead conductor rail (OCR), rigid overhead line, speed, span length, preload, pantograph, dynamic interaction.

## Abstract

The Overhead Conductor Rail is one of the methods to transmit energy to a moving train. This power feeding system has some advantages compared to the conventional overhead catenary system. However, its use is still mainly limited to underground and tunnel train infrastructures, probably due to a lack of knowledge of the performance of this method in some operating conditions. This work is devoted to the study of the influence of the speed, preload, and span length on the contact forces in the interaction between the pantograph and the overhead conductor rail. Three different lumped-element models of commercially available pantographs and a finite element model of

the overhead conductor rail have been used to carry out the simulations. The contact forces between each pantograph and the catenary have been obtained in all cases. The analysis of the results reveals that the higher the speed and span length are the higher the contact force fluctuations are. On the contrary, the increase in the preload leads to lower contact force oscillations provided no resonance effects are present.

## 1.- Introduction.

The Overhead Conductor Rail (OCR) system was patented in 1972 by the French firm Delachaux [1]. This power system has gained attraction in recent times. Recent studies have contributed to achieving a better knowledge of this power supply system for trains. However, despite these recent advances, its use is still mainly confined to tunnels for urban and suburban facilities. On one hand, OCR drawbacks are related to the scarce use of this system compared to conventional Overhead Catenary Systems (OCS). Among them, we can mention:

- poor performance at high speed
- higher initial cost of installation in open routes
- shorter span length
- less knowledge of the behaviour of this system compared to OCS

On the other hand, OCR has several advantages compared to the conventional Overhead Catenary System (OCS). Some of them are the following:

- greater robustness and lower maintenance costs
- reduced installation height requirements
- its large cross-section allows high electrical currents and better cooling in the event of overheating
- the absence of tensile forces allows greater use of the contact wire
- it avoids risk situations caused by the breaking of the contact wire in confined areas.

These advantages are relevant enough to consider OCR as a feasible solution in many new installations. However, a better knowledge of the performance of OCR and its interaction with the pantograph is required. Compared to OCS, fewer studies have been devoted to these kinds of facilities. In recent times, some research groups have been making big efforts to study the OCR to extend the use of this power feeding system. This paper is devoted to evaluating operational and design factors that have a big influence on the behaviour of OCR. These factors are speed, preload, and span length.

Most OCR facilities have been installed in low to medium speed rails. As mentioned before, the poor performance of pantograph-OCR interaction at high train speed is one of the most significant problems of this power feeding system. High vibration levels and contact force fluctuations are related to the increase in operational speed. This way, poor power transmission, and wear problems may arise under these conditions. The influence of operating speed on the quality of current collection in OCS has been widely tackled [[2]-[5]]. However, not many studies have focused on the study of this effect on OCR. For example, a more efficient OCR design with superior dynamic behaviour was described by C. Vera et al. [6]. These authors claimed that the proposed design led to an improved dynamic behaviour which consequently allowed higher running speeds. Similarly, a new rigid conductor line applicable to moderately high-speed operations was developed by Oya et al [7]. Mak Man [8] demonstrated the acceptable dynamic performance of an OCR facility for line operating speeds up to 130 km/h by conducting a simulation study of the interaction between the pantograph and

the OCR system. Finally, the contact forces between several pantograph models and two OCR sections at three different operating speeds were obtained in [9]. Recently, Furrer+Frey have tested their conductor rail at high speeds. A top speed of 302 km/h and 250 km/h of maximum operational speeds on some stretches were achieved [10]. Unfortunately, the results and measured data of these tests are neither publicly available nor have they been included in research papers. Despite these top speeds reached in some installations, OCR top speed is still well below OCS top speed.

The static contact force or preload is the mean vertical force exerted by the pantograph head on the OCR whilst the pantograph is raised and the train is at standstill. This static contact force is one of the main components of the dynamic contact force, i.e., the force exerted by the pantograph when the vehicle is moving. The dynamic contact force is a mean to evaluate the risk of the presence of electric arcs, sparking, and wear problems. Low values of dynamic contact force are related to the appearance of arcs and, as a consequence, to the deterioration of the contact wire and pantograph strips. The prediction of electric arcs is a challenging problem that requires very low sampling times and improved pantograph and catenary models. Consequently, the study of the formation of electric arcs during the interaction is out of the scope of this work. High levels of dynamic contact force lead to excessive wear and contact wire breakage. At present, the EN 50367 standard defines the limits for both the static and mean dynamic force for interoperability [11]. For instance, in [12][13] The influence of the static contact force on the pantograph-catenary interaction in OCS facilities was studied. However, to our knowledge, an in-depth study of the optimal preload condition for OCR has not been conducted yet. The aim of studying the influence of the preload on the overall performance of OCR is to contribute to determining the optimal value of this pre-fixed parameter in order to reduce wear problems and improve power feeding quality.

Finally, span length has also been tackled in some research papers. This way, Takemura et al installed a 100 m aluminum overhead rigid conductor and carried out tests to evaluate the influence on the current collection of span lengths between 5 to 9 meters [14]. More recently, Chen et al concluded that, among other factors, span length was a sensitive parameter that had a significant effect on the contact force [15].

Other research works about OCR have been devoted to studying simulation algorithms, wear-related problems, and maintenance. Thus, J.D Sanz proved that non-specific simulation software made it possible to study, with some limitations, highly complex problems like the dynamic interaction between pantograph and catenary. Nevertheless, several limitations were found when working with longer models in comparison with the use of specific simulation software [16]. A. Bautista presented an algorithm that resorted to co-simulation to reproduce the interaction between a catenary represented as a Finite Element Model and a pantograph modeled as a multibody linkage. The proposed algorithm, which proved to be fast and accurate, was intended to be a tool to optimize the design of infrastructure and pantograph [17]. Calleja et al developed a tuned mass damper prototype for rigid catenary systems [18]. The wear mechanisms, calculation and prediction, and the factors with a higher impact on the wear rate were tackled by Wei et al [19] and Guiming et al [20]. They concluded that, among other factors, the speed, contact pressure, temperature, and the presence of high vibration levels largely affect the wear of the pantograph strips and overhead line. Finally, Carnevale et al [21] developed a method to identify defects in a rigid overhead contact line. Simulations of a healthy and a defective line were carried out to find a meaningful index that allowed a robust identification of the defects.

Despite all these previous researches, further works are required to broaden the knowledge of this kind of facilities. Several challenges have to be solved yet to demonstrate the benefits and viability of installing such a system and to improve the

current collection quality between the pantograph and the OCR. This way, this paper is proposed as an approach to evaluate the performance of OCR facilities under different installation and operating conditions. Thus, in this paper, a previously validated Finite element OCR model is used to evaluate the influence of the span length, speed and preload on the contact forces in the catenary-pantograph interaction. Three span lengths: 8, 10 and 12 meters, four speeds: 70, 100, 130 and 160 km/h and four preload values: 70, 90, 110 and 130 N have been combined and simulated. Furthermore, three pantograph models have also been reproduced. Consequently, 144 simulations have been conducted in total, covering a broad range of possible OCR operating conditions.

The rest of this paper is structured as follows. Section 2 focuses on the description of the methodology followed to model the OCR-pantograph interaction. Pantograph models are described in subsection 2.1. OCR models are explained in subsection 2.2. The parameters of the interaction between the OCR and the pantograph and the definition of test conditions are presented in subsection 2.3. Next, a description of the studied cases is included in section 3. Results and discussions are shown in section 4. Section 5 is devoted to conclusions.

## 2.- OCR modelling

Models based on Finite Element Methods (FEM) are widely used to reproduce pantograph-catenary interaction [17][22][23][24]. Thus, following a similar approach adopted in previous works of this research group, the behaviour of the OCR has been reproduced in this paper by means of a finite element model [9][25]. In those works, the OCR consisted of beams of extruded aluminum profile type PAC 110 joined by flanges that accommodate a contact wire with a cross section of 150 mm2. The beams were fixed to bars with ceramic insulators on its extremes. These bars were supported by L-angle beams through two threaded rods. The whole structure was fixed to the tunnel ceiling by means of supports (see Figure 1).

**Figure 1. Profile type Pac 110 and support.**

In this paper, the aluminum profile and contact wire have been modelled as a ‘single body´ with a section and equivalent mechanical properties of the aluminum-copper assembly. This way, no clearance exists between these components. A 2-node beam element based on Timoshenko’s theory with element lengths of 0.2 m have been used. Flanges have been modelled with point elements with mass and rotary inertia. Finally, the supports that join the beam to the roof of the tunnel have been modelled using uniaxial tension-compression elements with constant stiffness. The implemented 2-D finite element model that reproduces OCR behaviour is shown in Figure 2.

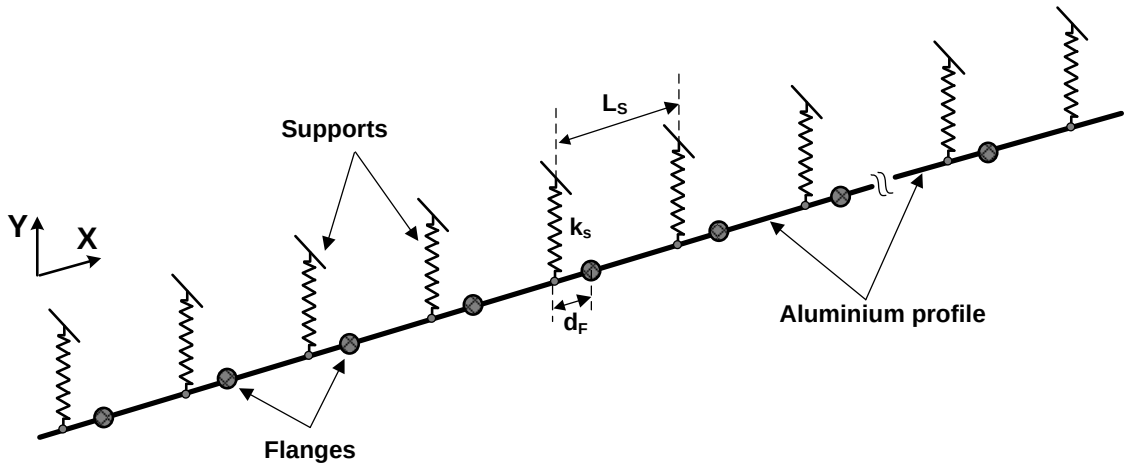


**Figure 2. OCR. Scheme of the finite element model of a rigid catenary installation.**

Where $k_S$ is the support stiffness, being the same for all supports, $d_F$ is the distance from the supports to the flanges and $L_S$ is the span length. Figure 3 shows a diagram of the section and the position of the supports. The values assigned to each parameter are also included in Figure 3. The X-axis points in the direction of train movement and the Y-axis points upward.

Next, the passsing of a train under a catenary stretch was reproduced to obtain the contact forces in the pantograph-catenary interaction. The catenary stretch was divided into two sections: initial section and test section. The total length of the modelled catenary stretch was 507.61 meters ($T_L$). The lengths of the initial and test sections were 120.65 and 390.5 meters respectively. An expansion joint was used to connect both sections. This expansion joint ensures a smooth mechanical and electrical transition of the pantograph between both sections. Three distances between supports of the catenary in the initial ($L_{IS}$) and test sections ($L_{TS}$) were simulated: 8, 10 and 12. Figure 3 shows a diagram of the section and the position of the supports. The number of supports in the test section was different depending on the distance between supports. This way, 51, 42 and 36 supports were required with 8, 10 and 12 meters of distance between supports respectively. Finally, the number of supports in the initial section was 17, 14 and 12 respectively.

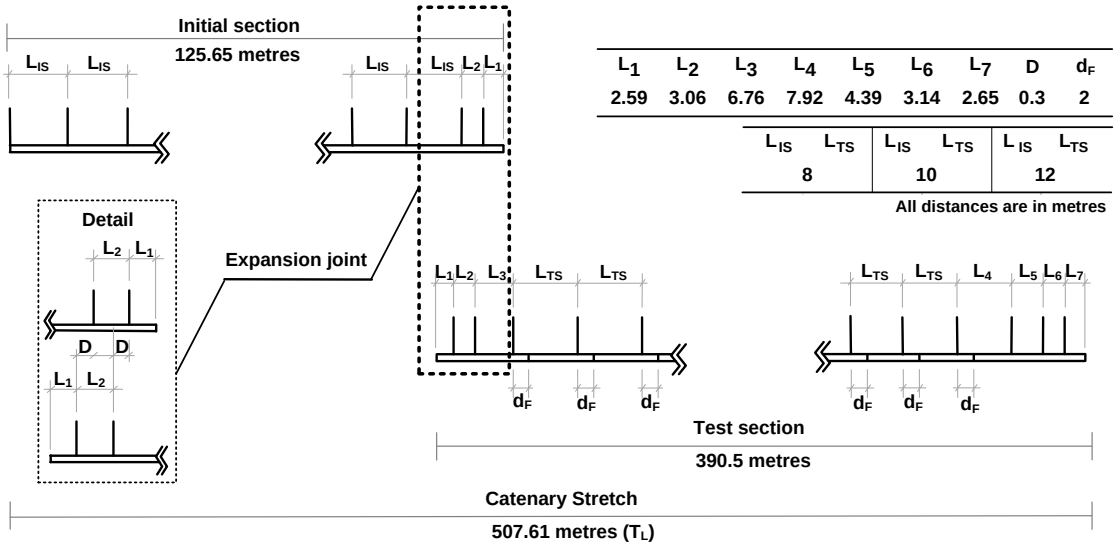


| $L_1$ | $L_2$ | $L_3$ | $L_4$ | $L_5$ | $L_6$ | $L_7$ | D | $d_F$ |
|---|---|---|---|---|---|---|---|---|
| 2.59 | 3.06 | 6.76 | 7.92 | 4.39 | 3.14 | 2.65 | 0.3 | 2 |

| $L_{IS}$ | $L_{TS}$ | $L_{IS}$ | $L_{TS}$ | $L_{IS}$ | $L_{TS}$ |
|---|---|---|---|---|---|
| 8 | | 10 | | 12 | |

**Figure 3. Scheme of the OCR section with support positions and flanges.**

The parameters that define the OCR finite element model used in this paper were obtained from experimental validation. This way, the validation of the finite element model of the support used in a real OCR facility installed in a tunnel of a commuter train in the city of Málaga (Spain) was carried out in a previous work of this research group [9]. Table 1 includes the main parameters of the OCR model used in the simulations conducted in this paper.

**Table 1. Parameters of the OCR finite element model in the test section.**

| | | Value | Units |
|---|---|---|---|
| **General** | Number of spans | 51, 42 and 36 | -- |
| | Span length | 8, 10 and 12 | m |
| **Aluminum profile and contact wire** | Equivalent section area | $2365 \times 10^{-6}$ | $m^2$ |
| | Equivalent inertia flexural property | $4.24678 \times 10^{-6}$ | $m^4$ |
| | Equivalent density | 3012.7 | $kg/m^3$ |
| | Young modulus | $6.9 \times 10^{10}$ | $N/m^2$ |
| **Flange** | Weight | 2.98 | kg |
| | Moment of inertia | $2.35 \times 10^{-3}$ | $kg\ m^2$ |
| **Support** | Support stiffness | 400000 | N/m |

## 3.- Pantograph modelling.

Several methods can be used to model pantograph behaviour. In some cases, multibody techniques [26][27] and flexible elements are successfully used [28][29][30]. However, in this paper, the pantographs are modelled using lumped elements (Figure 4). This technique is probably the most widely used and best-known method to reproduce the vertical movements of the pantograph [12][13][23][26][31][32][33]. This way, this work makes use of three pantograph models to evaluate the contact force in their interaction with an OCR.

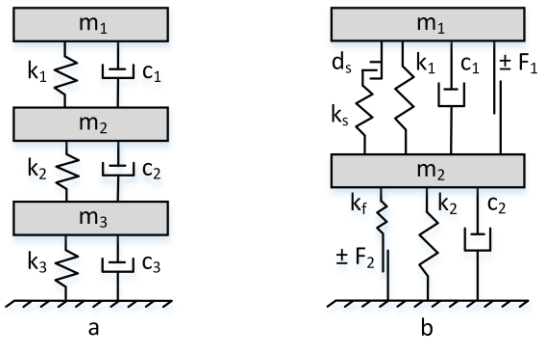


**Figure 4. Pantograph lumped-element models.**

Three and two degree-of-freedom (d.o.f.) pantograph models have been simulated (Figure 4a and 4b respectively). The first pantograph is described in [33]. It is composed of 9 mass-spring-damper lumped elements. Masses $m_1$, $m_2$ and $m_3$ represent the pan-head, upper frame and lower frame respectively. Next, a two d.o.f. pantograph model described in [13] has also been used. In this case, 7 lumped elements and two force saturations have been utilized. Masses $m_1$, and $m_2$ represent the pan-head and frame respectively. Finally, the third pantograph is similar to the first one except that it makes use of only one damper element, which is located between $m_1$ and $m_2$ [34]. Table 2 shows the values of masses, degrees of stiffness, and damping coefficients as well as the references in which these models are described.

**Table 2. Parameters of the different pantograph models.**

| | | Pantograph | | |
|---|---|---|---|---|
| **Parameter** | **Unit** | **P1 [33]** | **P2 [13]** | **P3 [34]** |
| $m_1$ | *kg* | 7,5 | 6 | 7,12 |
| $m_2$ | *kg* | 9 | 19,7 | 6 |
| $m_3$ | *kg* | 6 | - | 5,8 |
| $k_1$ | *N/m* | 7000 | 5800 | 9430 |
| $k_2$ | *N/m* | 15500 | - | 14100 |
| $k_3$ | *N/m* | 160 | - | 80 |
| $C_1$ | *Ns/m* | 45 | - | 0 |
| $C_2$ | *Ns/m* | 0,1 | 63,5 | 0 |
| $C_3$ | *Ns/m* | 100 | - | 70 |
| $F_1$ | *±N* | - | 4 | - |
| $F_2$ | *±N* | - | 3 | - |
| $k_F$ | *N/m* | - | 1e6 | - |
| $k_S$ | *N/m* | - | 1e6 | - |
| $d_S$ | *m* | - | 0,053 | - |

Additionally, Table 3 includes some relevant information about the studied pantographs, such as pantograph model, operational speed, and free pantograph natural frequencies. The resonant frequencies of the pantograph connected to the OCR with a contact stiffness of 50000 N/m have also been added. In this case,in the first ($f_{p1}$) and second ($f_{p2}$) modes of the three d.o.f. model, the pan-head movement is low, while the lower and upper frame oscillate in phase or in counter-phase respectively. Finally, the pan-head is oscillating while the upper and lower frame remain almost at rest in the third resonance mode ($f_{p3}$). These resonance modes are depicted in Figure 5. In the case of the two d.o.f. model, the frame oscillates and the pan-head is at rest at the frequency $f_{p1}$ and vice versa at the frequency $f_{p3}$.

**Table 3. Relevant information of the pantographs.**

| Pantograph / nomenclature | Model | Speed (km/h) | $f_{f1}$ (Hz) | $f_{f2}$ (Hz) | $f_{f3}$ (Hz) | $f_{p1}$ (Hz) | $f_{p2}$ (Hz) | $f_{p3}$ (Hz) |
|---|---|---|---|---|---|---|---|---|
| Pantograh 1 | ATR95 | 10 to 365 | 0.42 | 5.69 | 10.98 | 3.15 | 10.74 | 14.03 |
| Pantograh 2 | WBL | 250 (two pantographs) | 0.00 | 5.65 | --- | 2.58 | --- | 15.37 |
| Pantograh 3 | DSA380 | 250 and 300 | 0.33 | 6.57 | 12.31 | 3.85 | 11.55 | 14.98 |

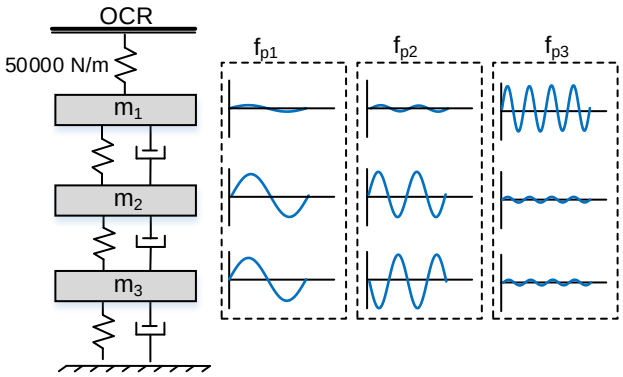


**Figure 5. Pantograh mode shapes.**

## 4.- OCR-Pantograph interaction modelling

The contact forces in the interaction between the OCR and the pantograph were obtained from finite element models using Ansys®. An outline of the modelling of this interaction is described next.

As mentioned before, three commercially available pantograph models were used in this study. Simulations were conducted to evaluate the influence of speed, preload and span length in the contact forces. This way, train speeds of 70, 100, 130 and 160 Km/h were reproduced. This range of speeds covers low speed to moderately high-speed applications. For each speed, four levels of preload were simulated, 70, 90, 110 and 130 N. Finally, span length influence was evaluated by performing simulations with 8, 10 and 12 m of distance between supports of the OCR.

The frequencies ($f_{ti\text{-}j}$, where i and j stand for the speed and span length respectively) at which the train passes under the supports have been included in Table 4.

**Table 4. Train passing excitation frequencies*.**

| | | Speed (km/h) | | | |
|---|---|---|---|---|---|
| **Span length** | | **70 Km/h** | **100 Km/h** | **130 Km/h** | **160 Km/h** |
| | **8 m** | 2.43 | 3.47 | 4.51 | 5.56 |
| | **10 m** | 1.94 | 2.78 | 3.61 | 4.44 |
| | **12 m** | 1.62 | 2.31 | 3.01 | 3.70 |

**Frequency in hertzs*

A contact stiffness of 50,000 N/m was considered to reproduce the contact between the pantograph head and the contact wire. Besides, no damping effect was reproduced in this contact. Regulation 50318:2003 only takes into account contact stiffness [35]. Besides, there is little, if any, information available on contact damping in the OCR. Numerical damping was used to stabilize numerical integration by means of a transient

integration parameter of a value equal to 0.005. The increase in train speed leads to a stronger interaction between the catenary and pantograph due to aerodynamic forces [26][32][36][37]. The contribution of this effect has been reproduced by adding an aerodynamic lift force ($F_{aero}$) proportional to the square of the train speed according to the following expression: $F_{aero} = F_{contact} + (0.000845 \cdot V^2)$, where $F_{contact}$ is the contact force in Newtons and $V$ is the train speed in Km/h. Gravity was introduced into the model to reproduce the presag of the catenary beams.

Figure 6 shows the OCR natural frequencies with the three modelled span lengths. The mounting natural frequencies are divided into two separated groups. The first is composed of the lowest frequencies, which are grouped between 5 to 10, 3 to 6.5 and 2 to 5 Hz for 8, 10 and 12 m. of span lengths respectively. Similarly, the second group includes resonant frequencies located between 16 to 19, 12 to 14 and 7 to 11 Hz. The horizontal lines indicate the train passing excitation frequencies ($f_t$), as shown in Table 4.

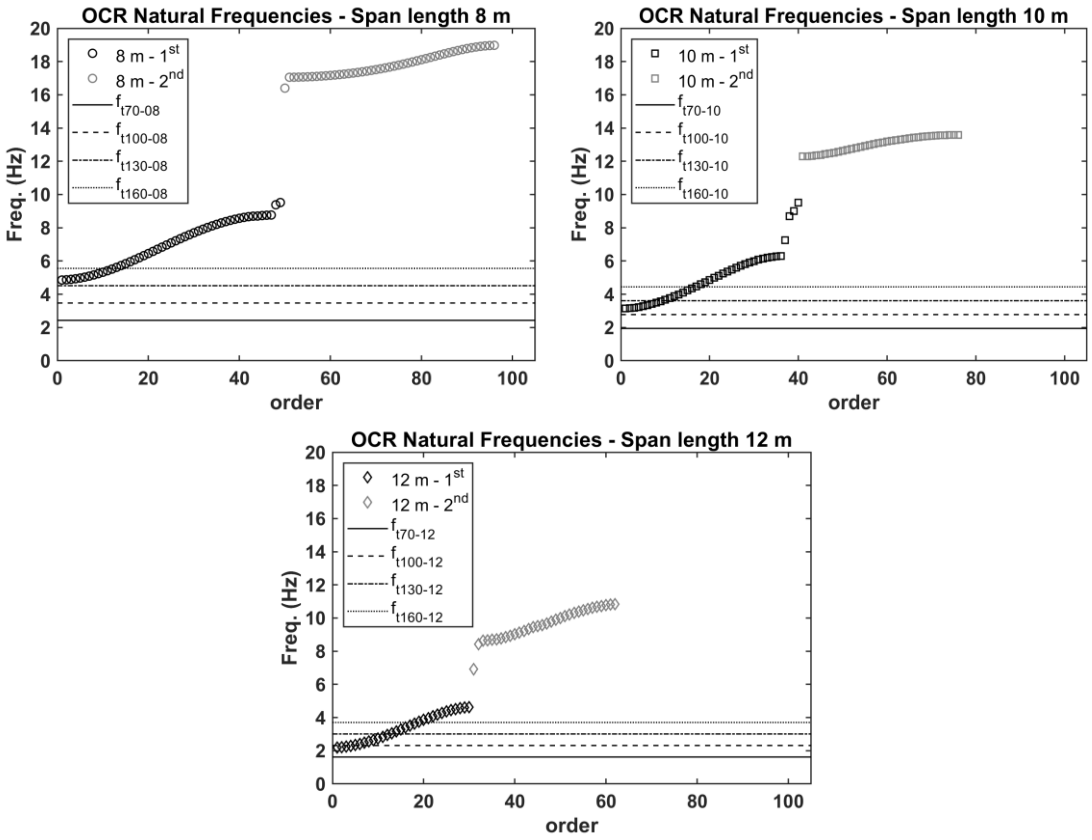


**Figure 6. OCR natural frequencies. Span length 8 m (top-left) - Span length 10 m (top-right) - Span length 12 m (bottom)**

As it can be seen, the frequencies of the excitations induced by the passing of the train barely excite the natural frequencies of the first group. However, with 10 and, especially, 12 meters of span length, the excitation caused by the train at medium and high speed are within the range of the first group of mounting natural frequencies. This fact might yield high vibration in the catenary and high fluctuations in the contact forces.

As mentioned before, the catenary stretch was divided into two sections. The first section, called initial section, was introduced to remove transient effects at the

beginning of train movement. Next, the train passed through the expansion joint and entered the second section, named test section. All simulations were performed following a sequential process. First, the effect of gravity was introduced and the preload force was set at the desired value. Next, the train was accelerated up to the required test speed. This transient process was conducted in the initial section. Then, the train passed through the expansion joint and entered the test section. Finally, the most relevant statistical values were calculated in a 275 m –length central stretch of the test section.

In these simulations, the influence of irregularities in the assembly of the supports of the rigid catenary has not been taken into account as well as irregularities due to repair and replacement of the contact wire, irregularities due to inhomogeneous wear of the contact strips and wire, and oscillations of the track. According to our knowledge, different irregularities influence contact forces on the interaction between the pantograph and the overhead conductor rail (OCR). Besides, not only irregularities in the assembly of the supports of the OCR generate variations in contact forces, but also local irregularities due to repair and replacement of the contact wire, irregularities in wear due to inhomogeneous wear of the contact strips, or even, oscillations of the track. However, according to [38, 39], it seems that this latter factor does not have a great influence on flexible catenary facilities. The study of the influence of assembly irregularities in flexible catenaries has been tackled in previously published works [5, 40-42]. Some of them foster the relevance of irregularities [40] while other approaches point out that irregularities are not a determining aspect in contact forces [5]. In addition, to the best of our knowledge, there are no published works that include experimental measures of irregularities in OCR facilities. Consequently, the influence of irregularities in contact forces has not been reproduced in this work. This way, this paper only focuses on the effect of speed, contact preload, span length, and the pantograph used on the contact forces. Furthermore, the inclusion of other factors might mask the influence of the selected factors. The authors are determined to evaluate the influence of irregularities in future studies.

The penalty method was adopted in this paper to obtain the contact forces between the pantograph and the catenary [34][43]. Contact forces were filtered with a 20 Hz cut-off frequency filter as recommended in EN 50367:2012 and EN 50317:2012 standards for experimental tests. A time step of 0.0025 s has been used in this work, which corresponds to 400 Hz. This time step was chosen according to the conclusions stated in [37]. A good balance between computational cost and result accuracy in all cases was observed for the chosen simulation time step. Simulations were carried out on an Intel(R) Core i7-8700K CPU, 3.7 GHz, 36 GB RAM, using ANSYS® 2019.

## 5.- Results.

As mentioned before, four speeds, four preload conditions and three span lengths were simulated. For each case, the maximum, minimum, average (mean) force and standard deviation were calculated. These values were obtained in a stretch of 275 m of the section located 60 m after the expansion joint. Main statistical values obtained in the simulations at 70, 100, 130 and 160 Km/h are included in Annexes A, B, C and D respectively.

### Simulation results at 70 km/h.

Figure 7 shows the forces obtained with pantograph 1 and 2 at a speed of 70 km/h, preload of 70 N and with a span length of 10 m. There are two shadowed areas in the figures. The first one corresponds to the expansion joint area. The second one is the stretch in which the statistical values and histograms are obtained.

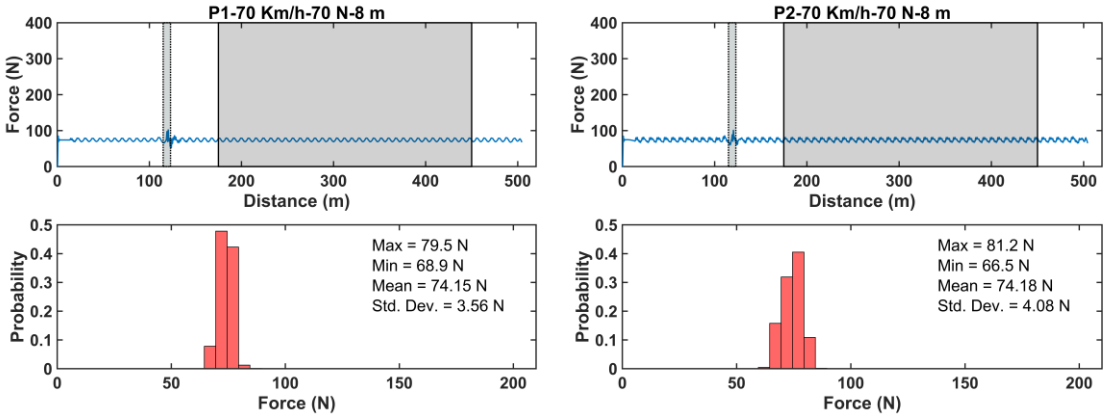


**Figure 7. Measured forces (top) and histogram (bottom). Pantograph 1 (left), pantograph 2 (right). 70 km/h.**

It can be seen that the mean force values are almost coincident with the nominal preload force. The measured forces are also well concentrated in a narrow band around the preload. The following plots show the distribution of forces in the measurement section for all the cases (Figure 8). The inferior and superior lines of the box are the 25$^{th}$ and 75$^{th}$ percentiles of the force data. The lower and upper hyphens indicate the lowest and largest data point excluding any outliers. The red crosses are measured data that are considered outliers. The line inside the box is the median of the force. Finally, the mean force is represented by a dot inside the box.

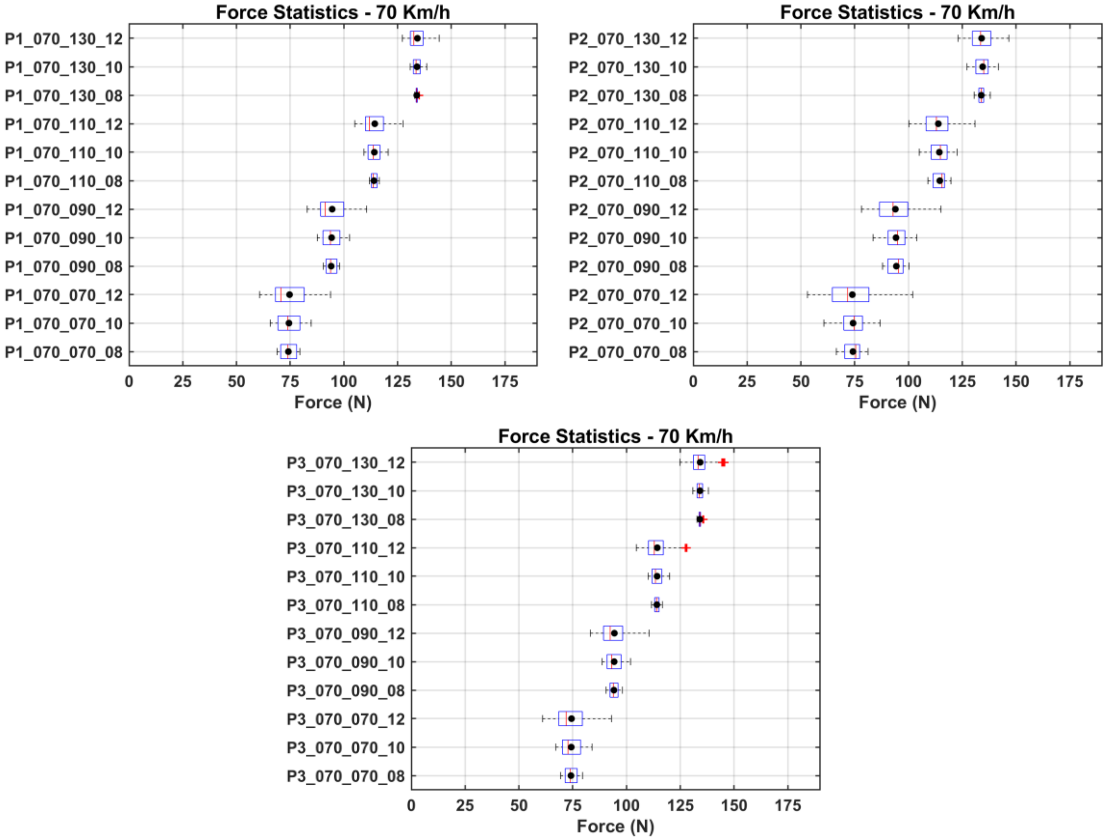


**Figure 8. Forces boxplot – 70 km/h.**

It can be seen that the longer the span length is, the larger the force fluctuations are. No pantograph-catenary separation is observed in any case. Finally, it seems that the variability of forces is slightly smaller in pantograph 3 compared to pantograph 1 and 2.

**Simulation results at 100 km/h**

Next, the results obtained in simulations carried out at 100 km/h are shown. Figure 9 shows the forces obtained with pantograph 1 and 2 at the speed of 100 km/h, preload of 90 N and with a span length of 12 m.

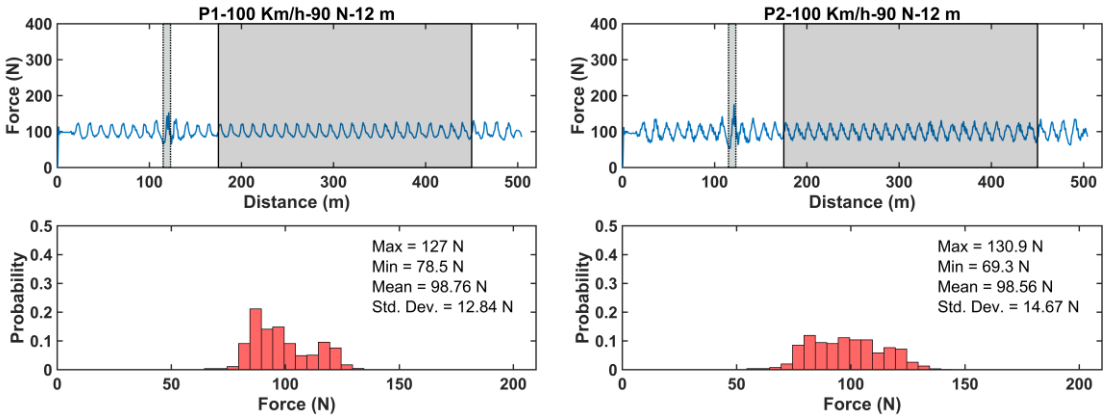


**Figure 9. Measured forces (top) and histograms (bottom). Pantograph 1 (left), pantograph 2 (right). 100 km/h.**

It can be observed that the increase in speed and, especially, in the span length has led to a wider distribution of the contact forces. The difference between the nominal preload and the mean force is due to the aerodynamic lift force acting on the pantograph. Pantographs 1 and 3 show a similar performance. However, the contact forces in pantograph 2 show slightly higher force fluctuations, being more noticeable when the span length is set at 12 m (Figure 10). The minimum force in the case of Pantograph 2 is close to being representative of a loss-of-contact condition in the lower preload case.

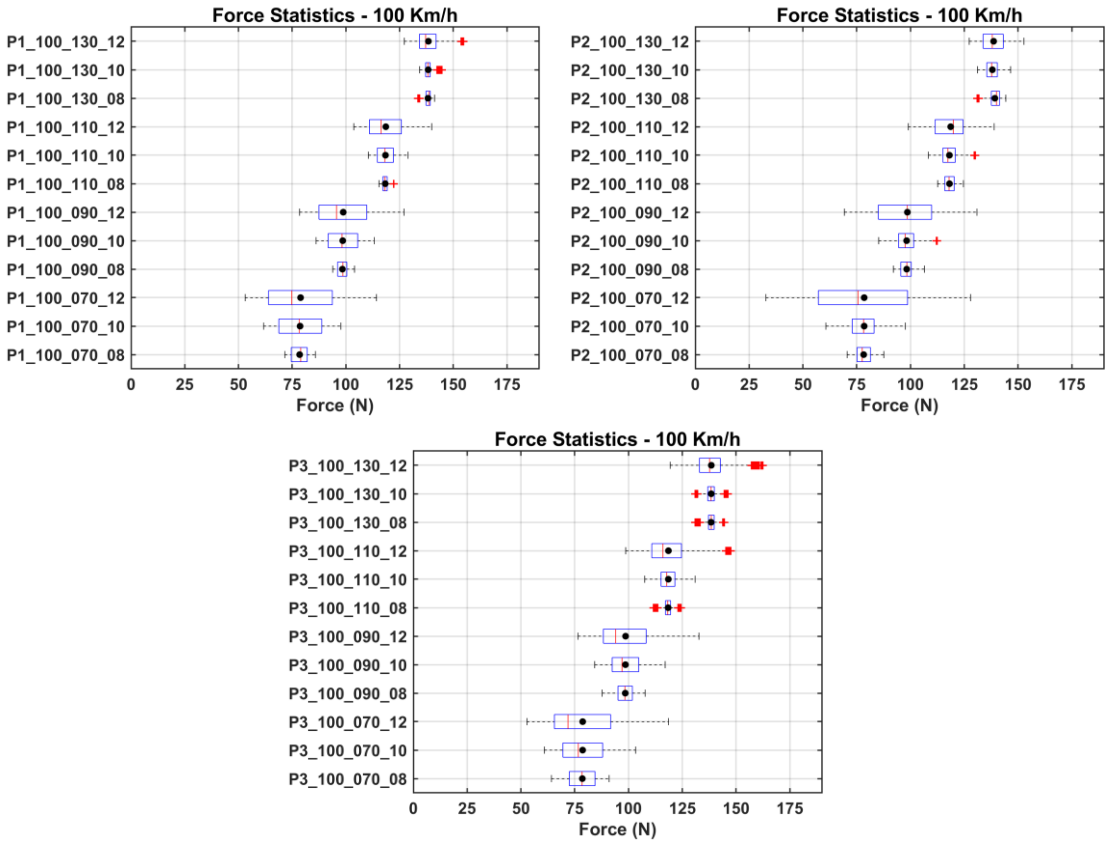


**Figure 10. Forces boxplot – 100 km/h.**

### 130 km/h

Figure 11 shows the forces obtained with pantograph 3 at the speed of 130 km/h, preload of 90 N and with a span length of 8, 10 and 12 m.

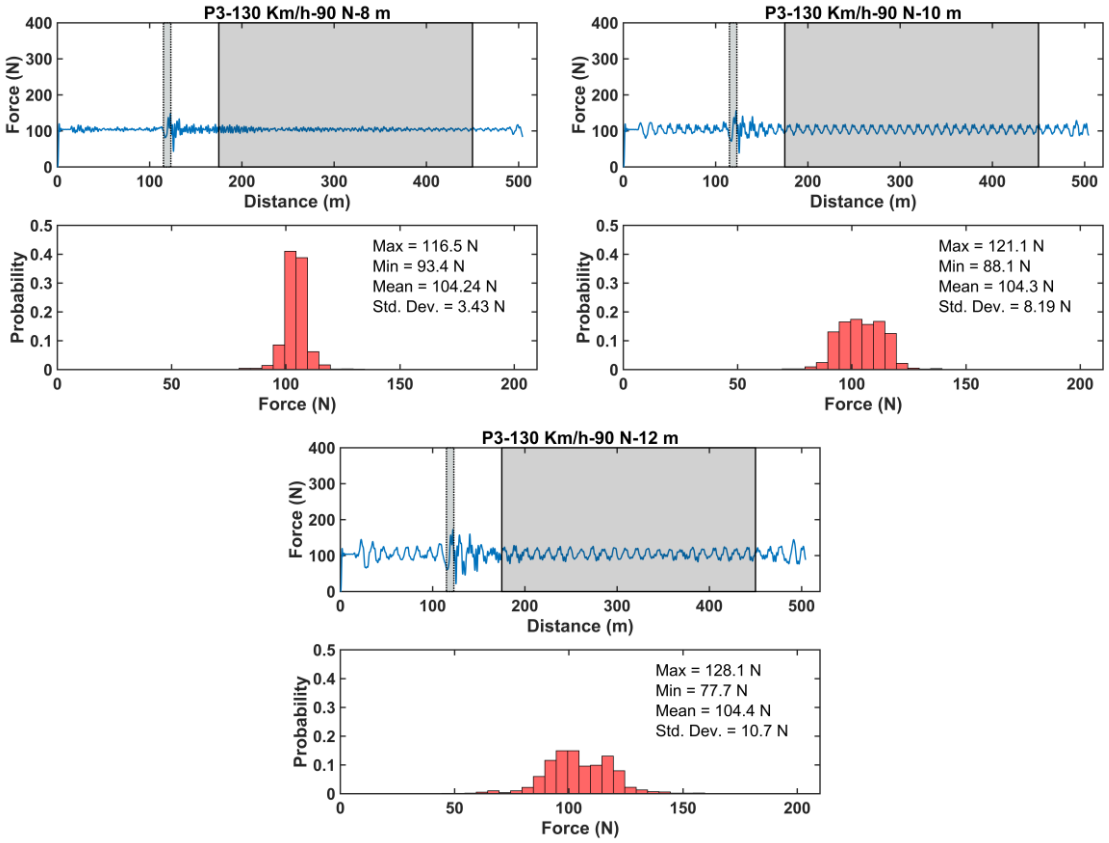


**Figure 11. Measured forces (top) and histograms (bottom). Pantograph 3. – 130 km/h.**

It can be seen that the increase in the span lengths leads to a worse performance of the pantograph-catenary interaction with a wider distribution of the contact forces, as shown in the forces histogram. Interestingly, the force oscillations in the area close to the expansion joint are also high in the 12 meter-span-length scenario. In this case, a loss of contact is close to taking place. In addition, the influence of the passing of the pantograph through the expansion joints is noticeable/remarkable up to 50 meters beyond the beginning of this joint.

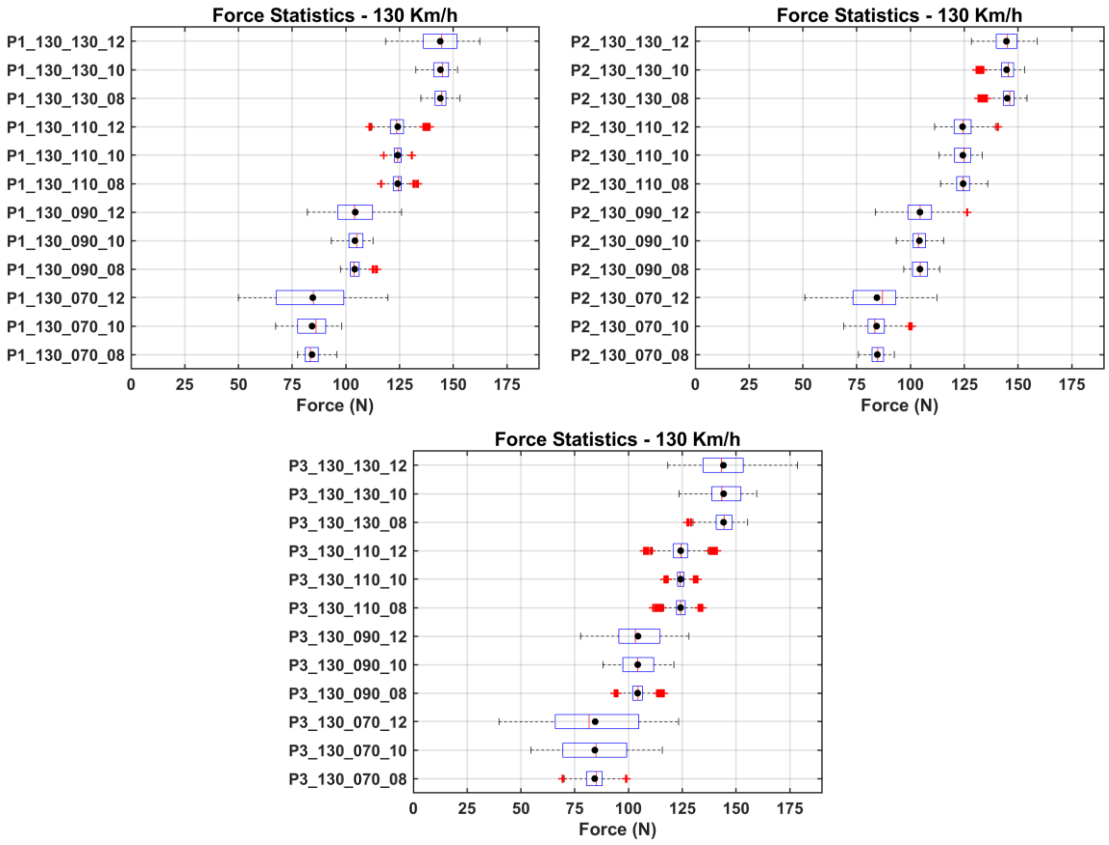


**Figure 12. Forces boxplot – 130 km/h.**

In this case, the higher force fluctuations are observed in pantograph 3. The performances of pantographs 1 and 2 are similar, again being poor in the case of the span length set at 12 m (Figure 12).

**160 km/h**

The following figures show the forces obtained with pantographs 1, 2 and 3 at the speed of 160 km/h, preload of 130 N and with a span length of 10 and 12 m (Figure 13 and Figure 14).

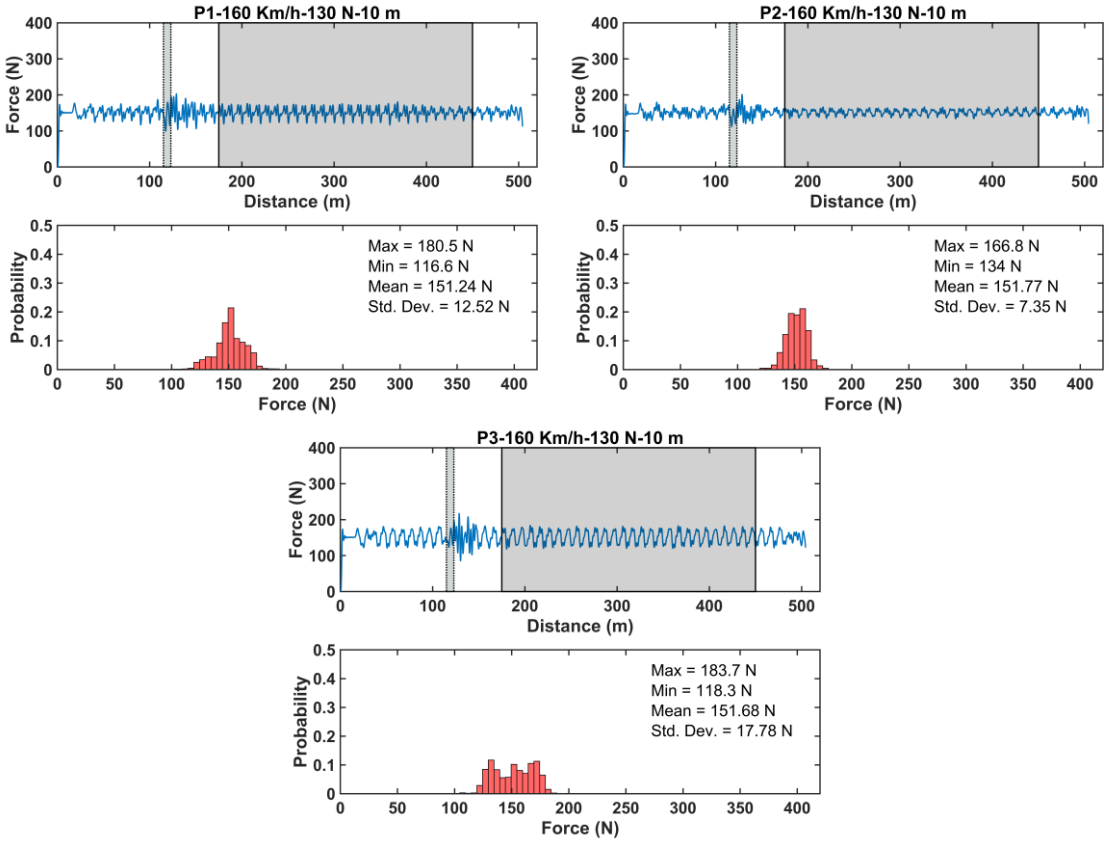


**Figure 13. Measured forces (top) and histograms (bottom). Pantograph 1 (top-left), pantograph 2 (top-right) and pantograph 3 (bottom-center). 160 km/h.**

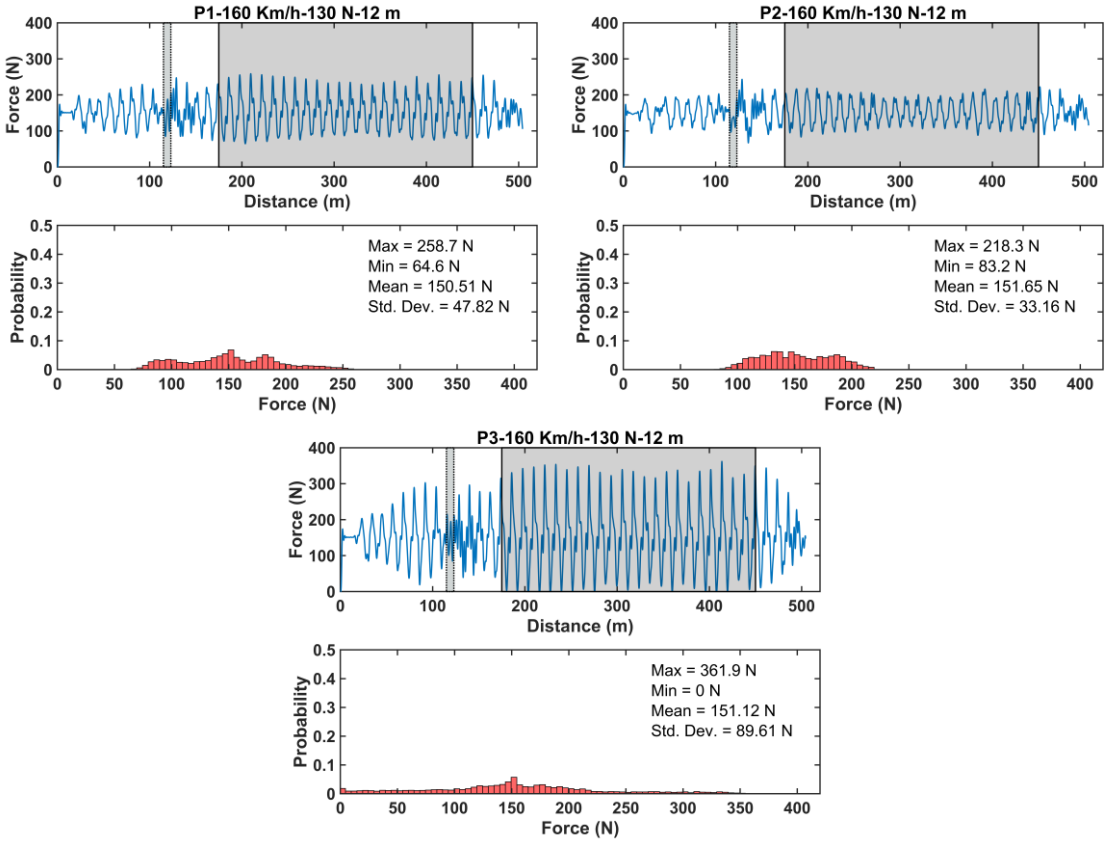

**Figure 14. Measured forces (top) and histograms (bottom). Pantograph 1 (top-left), pantograph 2 (top-right) and pantograph 3 (bottom-center). 160 km/h.**

Even though the mean forces are similar, it can be seen that the fluctuations of the forces are quite high in all cases (Figure 15). In the case of pantograph 3, high force fluctuations are observed even in the initial section before the expansion joint. Contact-loss conditions are detected due to the presence of resonances.

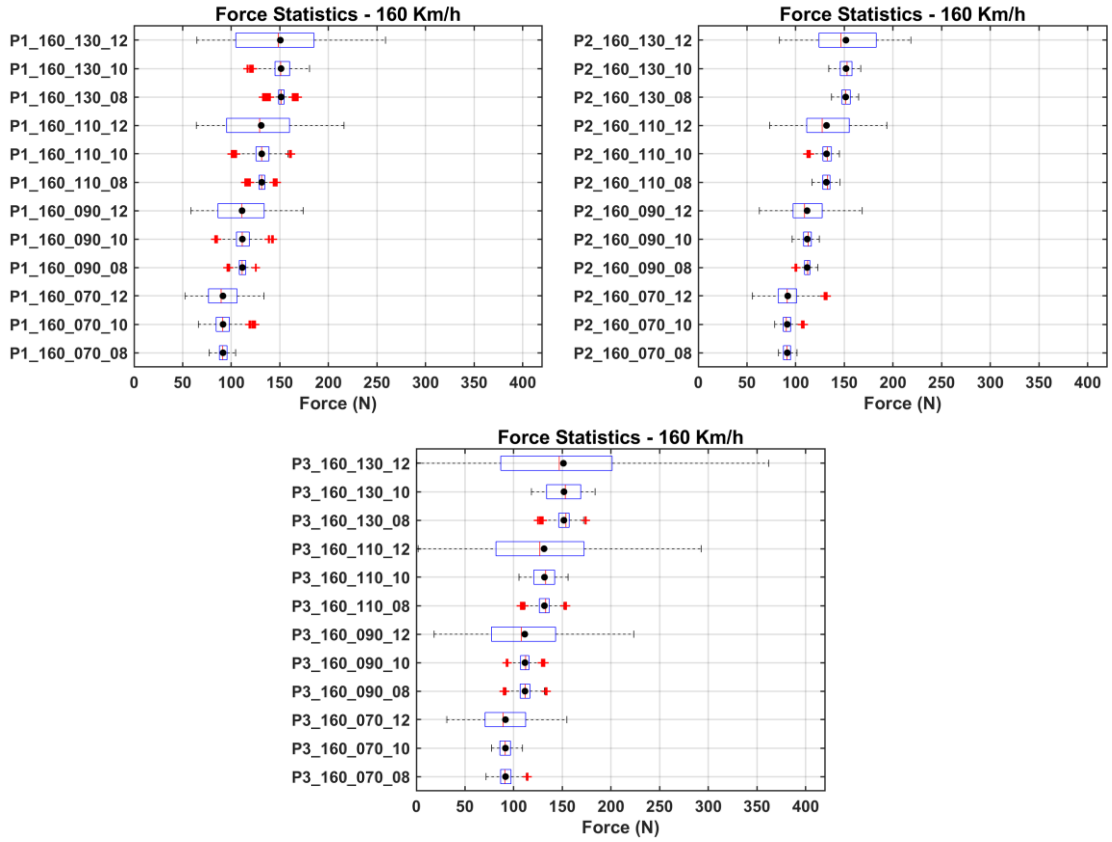


**Figure 15. Forces boxplot – 160 km/h.**

## 6.- Discussion

A profound study of the simulation results can help to gain better knowledge of these facilities. Thus, an analysis and a discussion of the results obtained from the interaction between the pantographs and the OCR in the cases described before is carried out next. Figure 16 to Figure 19 show the contact force standard deviations plotted versus the span length and the preload. In general terms, the following conclusions can be drawn:

- The higher the span length and speed are, the higher the force standard deviation is. This expected result is coincident with the general knowledge about this kind of facilities.
- The higher the preload is, the lower the force standard deviation is, except for tests conducted at 160 km/h.

As mentioned before, the higher the span length is, the higher the standard deviation is. A remarkable increase in the force standard deviations with a span length of 12 m compared with 8 and 10 m can be observed. According to [6], it is desirable for the standard deviation to be small, since a homogeneous contact force favours the current

collection process and reduces wear. This way, from the obtained results, it does not seem not to be advisable to increase the span length beyond 10 m. This conclusion coincides with the distances of most OCR facilities that have been installed so far. The choice between 8 and 10 meters of span length for a specific facility should be based on the operating conditions and the overall installation costs. This way, according to the results obtained in the studied cases with this OCR model, higher span length and low levels of preload can be appropriate if the facility is for low-speed operation conditions. On the other hand, as the speed increases the span length should be reduced.

Furthermore, results suggest that a reduction of the preload can be advisable since no contact-loss has been observed whatever the speed of the tests. This reduction in the preload force can reduce wear and other related effects. However, it would be necessary to perform experimental tests to validate this assumption. If so, specific regulations for OCR should be created to establish appropriate preload levels and operating conditions for these kinds of facilities. On the other hand, the reduction of the preload is associated with higher fluctuations in the contact forces for low and medium speed operation. The right balance between contact force, vibration and wear should be studied experimentally and/or using models that can reproduce the wear evolution related to the passing of the pantographs.

Forces obtained in the simulations carried out at the speed of 70 km/h show low amplitude oscillations. In all cases, the standard deviations of the measured forces are low whatever the preload conditions except for the case of pantograph 2 and the span length of 12 m, in which the highest fluctuations are observed. In this case, it seems that the best performance is achieved with pantograph 3. Similar conclusions can be drawn from tests conducted at 100 km/h.

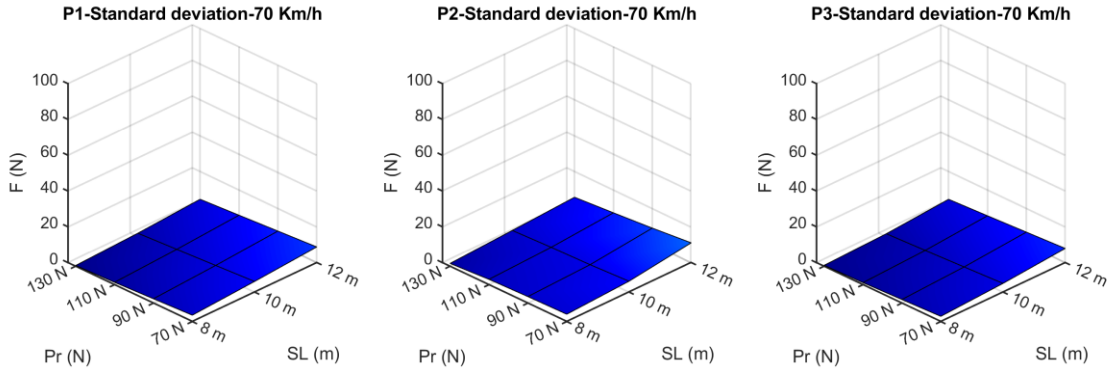


**Figure 16. Standard deviations vs span length (SL) and preload (Pr)- 70 km/h.**

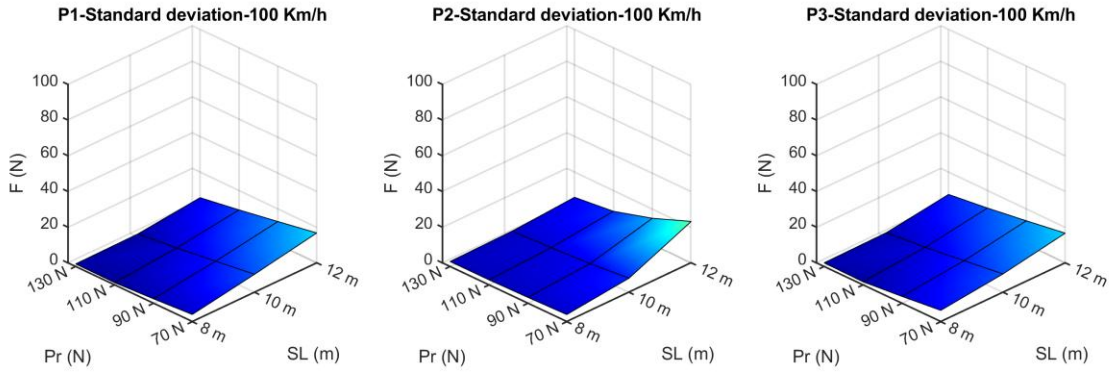


**Figure 17. Standard deviations vs span length (SL) and preload (Pr)- 100 km/h.**

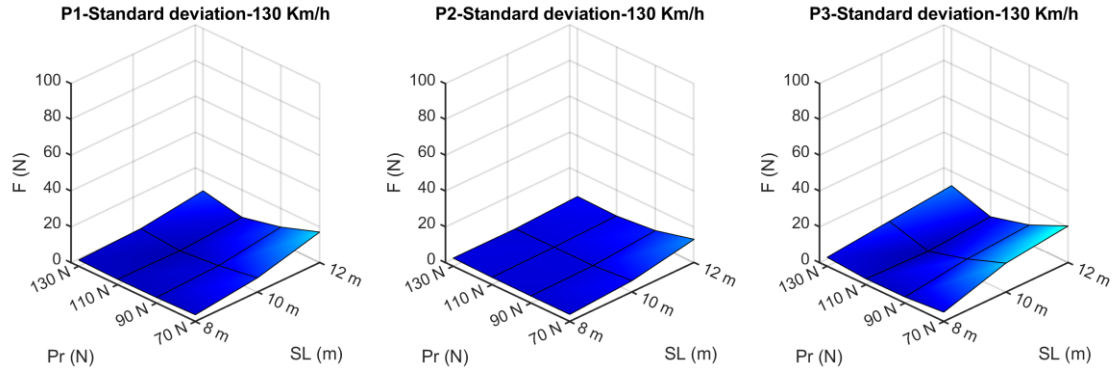


**Figure 18. Standard deviations vs span length (SL) and preload (Pr)- 130 km/h.**

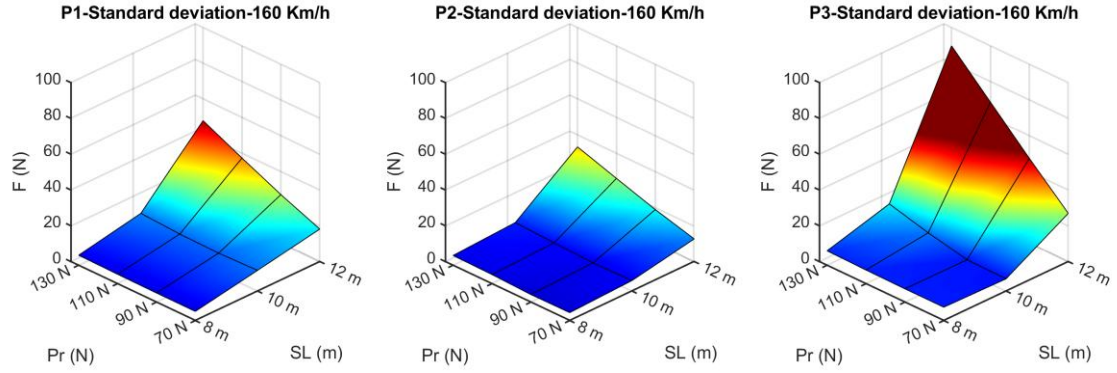


**Figure 19. Standard deviations vs span length (SL) and preload (Pr)- 160 km/h.**

Interestingly, it can be observed that, for some specific conditions, the force oscillations are considerably higher with some of the pantographs. Some examples of this situation can be found in tests included in Figure 20. This figure includes the amplitude spectrums of these tests. Harmonics of the train passing excitation frequency ($2xf_t$, $3xf_t$, $4xf_t$, and $5xf_t$), as well as pantograph resonant frequencies ($f_{p1}$, $f_{p2}$ and $f_{p3}$), have been indicated. Very high force standard deviations are observed in these cases. In particular, the worsts results were obtained at 160 km/h and span length of 12 m with pantograph 3. Measured forces were, in some cases, below 50 N and, in the case of pantograph 3, a contact-loss condition was detected. This fact is related to the resonance frequencies of the pantograph-OCR system. According to Figure 20, it can be seen that there is a huge increase in the vibration levels when the train passing excitation frequency ($f_t$) is close to the first resonant frequency ($f_{p1}$) of the connected pantograph. In the worst-case scenario, Pantograph 3, 12 m of span length and 160 km/h, harmonics 3 and 4 of the train passing frequency also excited pantograph resonance frequencies $f_{p2}$ and $f_3$, contributing to increasing de overall vibration level. Simulations conducted with and without damping showed that the influence of damping on the main statistical values could be considered negligible. This way, in the worst-case scenario, the influence of introducing damping on the standard deviation value is below 1.5%.

Moreover, it can also be observed that tests conducted at 130 km/h and a span length of 12 m. with pantograph 1 and 3 already show the initial effects of the presence of resonances. It can be seen that, in these cases, the standard deviation with a preload of 130 N is slightly higher compared to the standard deviation with 110 N of preload. This is an opposite effect of what can be observed in tests at lower speeds.

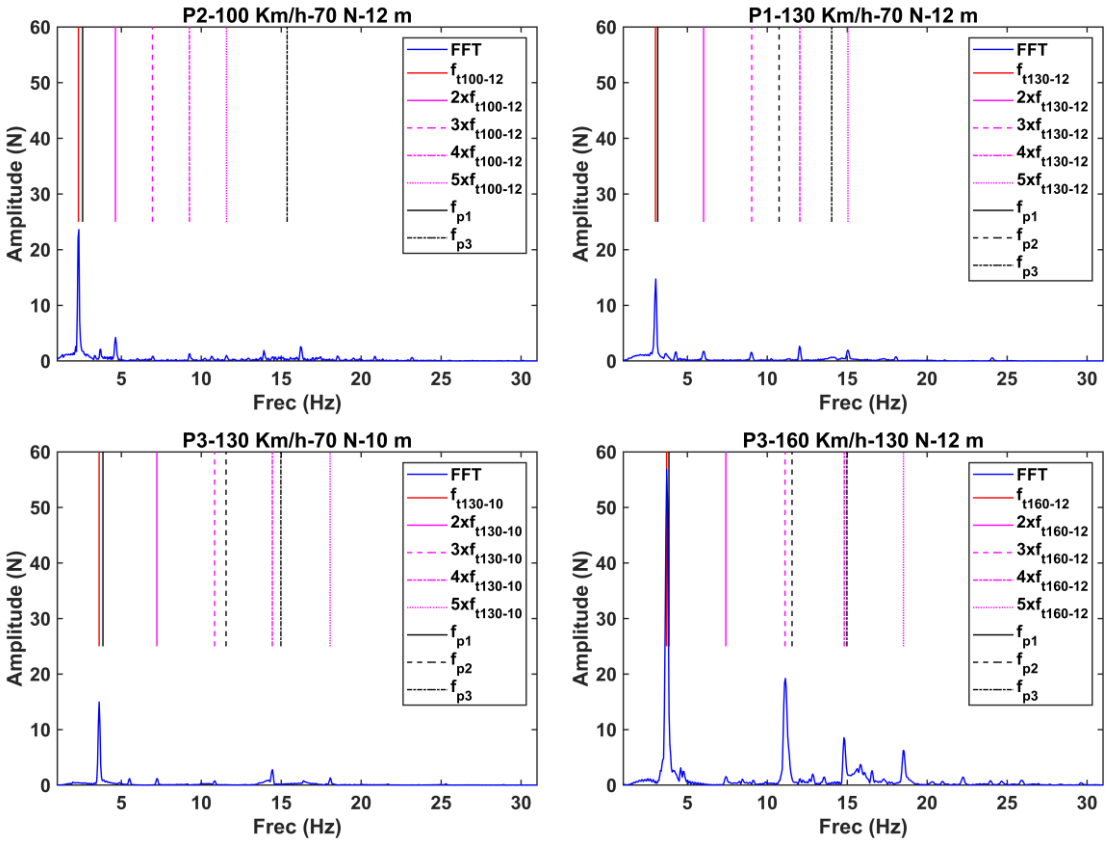


**Figure 20. Test spectrums.**

The combination of high speed and high span length has a noticeable influence on the vibration levels. As it can be seen in Figure 6, as the speed increases, the train passing frequency (Table 4) is more centered in the first group of OCR natural frequencies. This effect is more evident when the span length increases. This fact contributes to yielding higher vibration, mainly at low frequencies (2-5 Hz). The following figure shows an example of this phenomenon with the comparison of the spectrums obtained with pantograph 2, preload of 130 N, speed 160 km/h, and span lengths of 10 and 12 m. (Figure 21).

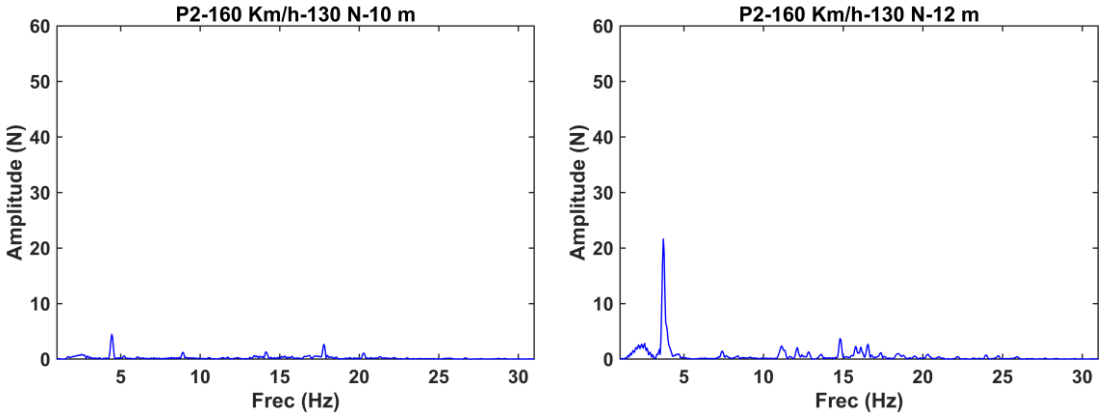


**Figure 21. Test spectrums.**

The influence of the expansion joint in the contact forces has also been shown. High force fluctuations were observed in the OCR stretch close to the expansion joint at 130 and 160 km/h. The effects of the passing of the pantograph along the expansion joints

were perceptible up to 50 meters beyond the initial contact point. This result might suggest that a change in the expansion joint design would be advisable.

Finally, Table 5 shows the standard deviations (σ) and forces measured and the limits for these values set by regulation EN 50367:2012 for tests conducted with 90 N of preload. It can be seen that, in all cases, the mean forces in the test section are within the limits set in that regulation. From this point of view, it seems that all configurations are acceptable. However, as shown in previous figures, the standard deviations of the forces are quite high in many cases. In fact, it does not fulfill the limit set in the regulation for the standard deviation in the last test. This result suggests that the combination of pantograph-catenary design and operating conditions are not satisfactory in those cases.

**Table 5. Standard deviation (σ) and mean forces and compariso with maximum standard deviation($\sigma_{max}$), maximum ($F_{m,max}$) and minimum forces ($F_{m,min}$) defined in regulation EN 50367:2012.**

| *Pantograph* | Test name | Speed (km/h) | Span length (m) | σ (N) | $\sigma_{max}$ $0.3*F_m$ (N) | Mean force (N) | $F_{m,max}$ (N) | $F_{m,min}$ (N) |
|---|---|---|---|---|---|---|---|---|
| *1* | P1_070_090_08 | 70 | 8 | 2.43 | 28,22 | 94.08 | 114.75 | 93.53 |
| | P1_070_090_10 | 70 | 10 | 4.57 | 28,29 | 94.29 | | |
| | P1_070_090_12 | 70 | 12 | 7.28 | 28,36 | 94.54 | | |
| | P1_100_090_08 | 100 | 8 | 2.53 | 29,51 | 98.38 | 119.70 | 97.20 |
| | P1_100_090_10 | 100 | 10 | 7.1 | 29,56 | 98.53 | | |
| | P1_100_090_12 | 100 | 12 | 12.84 | 29,63 | 98.76 | | |
| | P1_130_090_08 | 130 | 8 | 3.15 | 31,24 | 104.13 | 126.39 | 102.17 |
| | P1_130_090_10 | 130 | 10 | 4.48 | 31,26 | 104.21 | | |
| | P1_130_090_12 | 130 | 12 | 9.51 | 31,31 | 104.37 | | |
| | P1_160_090_08 | 160 | 8 | 5.11 | 33,44 | 111.45 | 134.83 | 108.43 |
| | P1_160_090_10 | 160 | 10 | 10.87 | 33,42 | 111.41 | | |
| | P1_160_090_12 | 160 | 12 | 27.09 | 33,33 | 111.11 | | |
| *2* | P2_070_090_08 | 70 | 8 | 3.65 | 28,31 | 94.35 | 114.75 | 93.53 |
| | P2_070_090_10 | 70 | 10 | 4.99 | 28,26 | 94.19 | | |
| | P2_070_090_12 | 70 | 12 | 8.93 | 28,17 | 93.91 | | |
| | P2_100_090_08 | 100 | 8 | 3.32 | 29,47 | 98.23 | 119.70 | 97.20 |
| | P2_100_090_10 | 100 | 10 | 5.74 | 29,46 | 98.2 | | |
| | P2_100_090_12 | 100 | 12 | 14.67 | 29,57 | 98.56 | | |
| | P2_130_090_08 | 130 | 8 | 3.97 | 31,32 | 104.39 | 126.39 | 102.17 |
| | P2_130_090_10 | 130 | 10 | 4.45 | 31,24 | 104.13 | | |
| | P2_130_090_12 | 130 | 12 | 7.56 | 31,31 | 104.38 | | |
| | P2_160_090_08 | 160 | 8 | 4.24 | 33,54 | 111.8 | 134.83 | 108.43 |
| | P2_160_090_10 | 160 | 10 | 5.44 | 33,58 | 111.93 | | |
| | P2_160_090_12 | 160 | 12 | 18.73 | 33,52 | 111.74 | | |
| *3* | P3_070_090_08 | 70 | 8 | 2.01 | 28,25 | 94.15 | 114.75 | 93.53 |
| | P3_070_090_10 | 70 | 10 | 3.73 | 28,28 | 94.27 | | |
| | P3_070_090_12 | 70 | 12 | 6.69 | 28,31 | 94.37 | | |
| | P3_100_090_08 | 100 | 8 | 3.88 | 29,55 | 98.49 | 119.70 | 97.20 |
| | P3_100_090_10 | 100 | 10 | 7.36 | 29,58 | 98.59 | | |
| | P3_100_090_12 | 100 | 12 | 13.25 | 29,59 | 98.64 | | |
| | P3_130_090_08 | 130 | 8 | 3.43 | 31,27 | 104.24 | 126.39 | 102.17 |
| | P3_130_090_10 | 130 | 10 | 8.19 | 31,29 | 104.3 | | |
| | P3_130_090_12 | 130 | 12 | 10.7 | 31,32 | 104.4 | | |
| | P3_160_090_08 | 160 | 8 | 7.43 | 33,48 | 111.61 | 134.83 | 108.43 |
| | P3_160_090_10 | 160 | 10 | 7.2 | 33,48 | 111.59 | | |
| | P3_160_090_12 | 160 | 12 | **47.35** | 33,42 | 111.4 | | |

## 7.- Conclusions

In this work, the influence of speed, preload, and span length on the forces between the OCR and the pantograph has been studied. The models of three commercially available pantographs have been programmed. Four different speeds, four preload conditions, and three span lengths have been simulated. This way, a total of 144 tests have been carried out. They represent low to moderately high speed operating conditions, recommended test preload values and two values above the recommended one, and span lengths representative of real facilities. Simulations were carried out using a validated finite element model of the OCR.

Results suggest that the higher the span length and the speed are, the higher the contact force fluctuations are. On the contrary, higher preloads contribute to a more homogenous contact force. However, higher preloads are also associated with higher contact wire wear rates, so a decision should be made to determine the best-operating conditions.

It has also been observed that if the OCR natural frequencies are excited by the pantograph passing, a dramatic increase in the contact force standard deviation takes place, leading to contact-loss. Therefore, this condition should be studied in advance to prevent future poor operating conditions.

Finally, results suggest that a proper selection of the pantograph according to the operating conditions is advisable, since the three studied models show that huge performance differences are observed, depending on the speed of the train and the length of the span. Similarly, it has been shown that expansion joints also have a big influence on the performance of the OCR-pantograph operation at higher speeds.

The main contributions of this paper are summarized as follows:

- Contact forces in the interaction between the catenary and pantograph have been obtained.
- Three commercially available pantographs have been modelled and the contact forces between each one of them and the OCR have been simulated.
- The influence of span length, preload and train speed on contact forces has been characterized.
- Obtained results have been analyzed. Results confirm well-known experimental observations but they also contribute to getting insights into the reasons that cause high changes in contact forces.

All in all, they can contribute to helping to improve the design of OCR facilities and to decide the best operational conditions by infrastructure administrators.

Future works will be focused on the evaluation of the performance of a wider range of pantographs and on studying the best pantograph model parameters for each facility. Furthermore, on-field tests should be conducted to validate the results suggested in this paper. In addition, the evaluation of the influence of the studied parameters on the wear rate of OCR facilities will also be tackled in future papers. Future works will also include the influence of contact wire irregularities and incorrect positioning of supports.

## Annex A: Main statistical values – Tests 70 km/h

| *Pantograph* | Test name | Preload (N) | Span length (m) | Maximum force (N) | Minimum force (N) | Mean force (N) | Median (N) | Standard Deviation (N) |
|---|---|---|---|---|---|---|---|---|
| *1* | P1_070_070_08 | 70 | 8 | 79.5 | 68.9 | 74.15 | 73.91 | 3.56 |
| | P1_070_070_10 | 70 | 10 | 84.8 | 65.7 | 74.42 | 73.85 | 5.91 |
| | P1_070_070_12 | 70 | 12 | 93.8 | 60.7 | 74.7 | 70.63 | 8.72 |
| | P1_070_090_08 | 90 | 8 | 98 | 90.4 | 94.08 | 93.8 | 2.43 |
| | P1_070_090_10 | 90 | 10 | 102.7 | 87.6 | 94.29 | 93.73 | 4.57 |
| | P1_070_090_12 | 90 | 12 | 110.6 | 82.9 | 94.54 | 91.26 | 7.28 |
| | P1_070_110_08 | 110 | 8 | 116.5 | 111.9 | 114.01 | 113.66 | 1.33 |
| | P1_070_110_10 | 110 | 10 | 120.6 | 109.3 | 114.18 | 113.67 | 3.25 |
| | P1_070_110_12 | 110 | 12 | 127.5 | 105 | 114.38 | 111.88 | 5.85 |
| | P1_070_130_08 | 130 | 8 | 135 | 132.9 | 133.92 | 133.89 | 0.4 |
| | P1_070_130_10 | 130 | 10 | 138.6 | 130.9 | 134.05 | 133.62 | 1.96 |
| | P1_070_130_12 | 130 | 12 | 144.4 | 127.2 | 134.24 | 132.55 | 4.45 |
| *2* | P2_070_070_08 | 70 | 8 | 81.2 | 66.5 | 74.18 | 75.46 | 4.08 |
| | P2_070_070_10 | 70 | 10 | 86.8 | 60.7 | 74.24 | 74.72 | 6.04 |
| | P2_070_070_12 | 70 | 12 | 102 | 53 | 73.9 | 71.72 | 11.02 |
| | P2_070_090_08 | 90 | 8 | 100.3 | 87.9 | 94.35 | 95.33 | 3.65 |
| | P2_070_090_10 | 90 | 10 | 103.8 | 83.5 | 94.19 | 94.87 | 4.99 |
| | P2_070_090_12 | 90 | 12 | 115.1 | 78.2 | 93.91 | 92.82 | 8.93 |
| | P2_070_110_08 | 110 | 8 | 119.7 | 109 | 114.55 | 115.53 | 2.98 |
| | P2_070_110_10 | 110 | 10 | 122.6 | 105 | 114.34 | 114.81 | 4.38 |
| | P2_070_110_12 | 110 | 12 | 130.9 | 100.2 | 113.87 | 112.97 | 7.19 |
| | P2_070_130_08 | 130 | 8 | 138 | 130.5 | 133.81 | 133.81 | 1.57 |
| | P2_070_130_10 | 130 | 10 | 141.8 | 127.2 | 134.47 | 134.97 | 3.5 |
| | P2_070_130_12 | 130 | 12 | 146.6 | 123 | 133.98 | 133.51 | 5.58 |
| *3* | P3_070_070_08 | 70 | 8 | 79.6 | 69.4 | 74.18 | 73.84 | 2.91 |
| | P3_070_070_10 | 70 | 10 | 84 | 67.1 | 74.34 | 72.81 | 4.83 |
| | P3_070_070_12 | 70 | 12 | 93 | 61 | 74.44 | 71.96 | 7.89 |
| | P3_070_090_08 | 90 | 8 | 98.1 | 90.5 | 94.15 | 93.9 | 2.01 |
| | P3_070_090_10 | 90 | 10 | 101.9 | 88.7 | 94.27 | 93.07 | 3.73 |
| | P3_070_090_12 | 90 | 12 | 110.5 | 83.2 | 94.37 | 92.41 | 6.69 |
| | P3_070_110_08 | 110 | 8 | 116.7 | 111.6 | 114.12 | 114.04 | 1.14 |
| | P3_070_110_10 | 110 | 10 | 120 | 110 | 114.22 | 113.45 | 2.66 |
| | P3_070_110_12 | 110 | 12 | 127.9 | 104.6 | 114.3 | 112.91 | 5.53 |
| | P3_070_130_08 | 130 | 8 | 135.8 | 132.7 | 134.08 | 134.09 | 0.5 |
| | P3_070_130_10 | 130 | 10 | 138.1 | 130.8 | 134.16 | 133.89 | 1.66 |
| | P3_070_130_12 | 130 | 12 | 145.6 | 124.8 | 134.24 | 133.29 | 4.44 |

## Annex B: Main statistical values – Tests 100 km/h

| *Pantograph* | Test name | Preload (N) | Span length (m) | Maximum force (N) | Minimum force (N) | Mean force (N) | Median (N) | Standard Deviation (N) |
|---|---|---|---|---|---|---|---|---|
| *1* | P1_100_070_08 | 70 | 8 | 85.8 | 71.5 | 78.47 | 78.96 | 4.03 |
| | P1_100_070_10 | 70 | 10 | 97.7 | 61.7 | 78.66 | 78.28 | 10.07 |
| | P1_100_070_12 | 70 | 12 | 114.3 | 53.1 | 78.9 | 74.81 | 16.74 |
| | P1_100_090_08 | 90 | 8 | 104 | 93.9 | 98.38 | 98.62 | 2.53 |
| | P1_100_090_10 | 90 | 10 | 113.2 | 86.1 | 98.53 | 98.2 | 7.1 |
| | P1_100_090_12 | 90 | 12 | 127 | 78.5 | 98.76 | 95.63 | 12.84 |
| | P1_100_110_08 | 110 | 8 | 122.3 | 115.4 | 118.31 | 118.16 | 1.29 |
| | P1_100_110_10 | 110 | 10 | 128.9 | 110.5 | 118.43 | 118.13 | 4.2 |
| | P1_100_110_12 | 110 | 12 | 139.9 | 103.7 | 118.58 | 116.36 | 9.05 |
| | P1_100_130_08 | 130 | 8 | 141.3 | 133.5 | 138.21 | 138.61 | 1.45 |
| | P1_100_130_10 | 130 | 10 | 144.6 | 134.3 | 138.3 | 138.19 | 1.76 |
| | P1_100_130_12 | 130 | 12 | 154.7 | 127.2 | 138.41 | 137.13 | 5.6 |
| *2* | P2_100_070_08 | 70 | 8 | 87.6 | 70.6 | 78.24 | 77.57 | 3.98 |
| | P2_100_070_10 | 70 | 10 | 97.6 | 60.7 | 78.46 | 78.2 | 7.86 |
| | P2_100_070_12 | 70 | 12 | 127.9 | 32.8 | 78.47 | 75.59 | 23.2 |
| | P2_100_090_08 | 90 | 8 | 106.4 | 92 | 98.23 | 98.29 | 3.32 |
| | P2_100_090_10 | 90 | 10 | 112.4 | 85.2 | 98.2 | 97.53 | 5.74 |
| | P2_100_090_12 | 90 | 12 | 130.9 | 69.3 | 98.56 | 98.51 | 14.67 |
| | P2_100_110_08 | 110 | 8 | 124.6 | 112.6 | 118.12 | 117.93 | 2.84 |
| | P2_100_110_10 | 110 | 10 | 130.1 | 108.3 | 118.09 | 117.38 | 4.34 |
| | P2_100_110_12 | 110 | 12 | 138.9 | 99 | 118.68 | 119.9 | 8.27 |
| | P2_100_130_08 | 130 | 8 | 144.3 | 131 | 139.21 | 139.94 | 2.79 |
| | P2_100_130_10 | 130 | 10 | 146.5 | 131.1 | 138.05 | 137.7 | 3.37 |
| | P2_100_130_12 | 130 | 12 | 152.7 | 127.3 | 138.63 | 138.01 | 5.82 |
| *3* | P3_100_070_08 | 70 | 8 | 91 | 64.2 | 78.55 | 78.42 | 6.33 |
| | P3_100_070_10 | 70 | 10 | 103.3 | 60.9 | 78.68 | 76.68 | 10.28 |
| | P3_100_070_12 | 70 | 12 | 118.6 | 52.8 | 78.71 | 71.88 | 16.63 |
| | P3_100_090_08 | 90 | 8 | 107.7 | 87.8 | 98.49 | 98.32 | 3.88 |
| | P3_100_090_10 | 90 | 10 | 117 | 84.3 | 98.59 | 96.99 | 7.36 |
| | P3_100_090_12 | 90 | 12 | 132.7 | 76.5 | 98.64 | 94.02 | 13.25 |
| | P3_100_110_08 | 110 | 8 | 124.4 | 111.6 | 118.42 | 118.24 | 1.76 |
| | P3_100_110_10 | 110 | 10 | 131 | 107.5 | 118.52 | 117.75 | 4.57 |
| | P3_100_110_12 | 110 | 12 | 147.6 | 98.7 | 118.56 | 116 | 10.09 |
| | P3_100_130_08 | 130 | 8 | 144.5 | 130.9 | 138.37 | 138.47 | 2.06 |
| | P3_100_130_10 | 130 | 10 | 146.2 | 131 | 138.43 | 138.37 | 2.46 |
| | P3_100_130_12 | 130 | 12 | 162.4 | 119.4 | 138.48 | 137.69 | 7.41 |

## Annex C: Main statistical values – Tests 130 km/h

| *Pantograph* | Test name | Preload (N) | Span length (m) | Maximum force (N) | Minimum force (N) | Mean force (N) | Median (N) | Standard Deviation (N) |
|---|---|---|---|---|---|---|---|---|
| *1* | P1_130_070_08 | 70 | 8 | 95.8 | 77.5 | 84.22 | 83.47 | 3.77 |
| | P1_130_070_10 | 70 | 10 | 98 | 67.3 | 84.26 | 86.11 | 7.94 |
| | P1_130_070_12 | 70 | 12 | 119.5 | 50 | 84.59 | 84.87 | 17.03 |
| | P1_130_090_08 | 90 | 8 | 114.7 | 97.5 | 104.13 | 103.73 | 3.15 |
| | P1_130_090_10 | 90 | 10 | 112.6 | 93.2 | 104.21 | 105.04 | 4.48 |
| | P1_130_090_12 | 90 | 12 | 125.9 | 82 | 104.37 | 104.08 | 9.51 |
| | P1_130_110_08 | 110 | 8 | 133.7 | 116.3 | 124.08 | 124.52 | 3.03 |
| | P1_130_110_10 | 110 | 10 | 130.8 | 117.6 | 124.12 | 124.12 | 2.44 |
| | P1_130_110_12 | 110 | 12 | 139.1 | 110.9 | 124.15 | 123.67 | 4.67 |
| | P1_130_130_08 | 130 | 8 | 153.1 | 134.9 | 143.99 | 144.65 | 3.48 |
| | P1_130_130_10 | 130 | 10 | 152 | 132.6 | 144.04 | 144.89 | 4.53 |
| | P1_130_130_12 | 130 | 12 | 162.3 | 118.4 | 143.93 | 144.65 | 9.19 |
| *2* | P2_130_070_08 | 70 | 8 | 92.5 | 75.8 | 84.59 | 84.77 | 3.95 |
| | P2_130_070_10 | 70 | 10 | 100.7 | 69 | 84.23 | 83.44 | 6.31 |
| | P2_130_070_12 | 70 | 12 | 112.3 | 50.9 | 84.38 | 86.97 | 12.98 |
| | P2_130_090_08 | 90 | 8 | 113.5 | 96.9 | 104.39 | 104.51 | 3.97 |
| | P2_130_090_10 | 90 | 10 | 115.4 | 93.4 | 104.13 | 103.66 | 4.45 |
| | P2_130_090_12 | 90 | 12 | 126.5 | 83.7 | 104.38 | 104.47 | 7.56 |
| | P2_130_110_08 | 110 | 8 | 135.9 | 113.9 | 124.46 | 124.38 | 4.11 |
| | P2_130_110_10 | 110 | 10 | 133.3 | 113.2 | 124.34 | 124.89 | 4.51 |
| | P2_130_110_12 | 110 | 12 | 140.8 | 111.2 | 124.2 | 124.45 | 5.45 |
| | P2_130_130_08 | 130 | 8 | 154.1 | 131.5 | 144.96 | 146.13 | 4.54 |
| | P2_130_130_10 | 130 | 10 | 153 | 130.5 | 144.66 | 145.51 | 4.42 |
| | P2_130_130_12 | 130 | 12 | 158.9 | 128.3 | 144.59 | 145.09 | 6.03 |
| *3* | P3_130_070_08 | 70 | 8 | 99.1 | 69.3 | 84.28 | 85.1 | 5.23 |
| | P3_130_070_10 | 70 | 10 | 115.7 | 54.6 | 84.35 | 84.87 | 16.15 |
| | P3_130_070_12 | 70 | 12 | 123.3 | 39.8 | 84.51 | 81.67 | 20.42 |
| | P3_130_090_08 | 90 | 8 | 116.5 | 93.4 | 104.24 | 104.42 | 3.43 |
| | P3_130_090_10 | 90 | 10 | 121.1 | 88.1 | 104.3 | 104.18 | 8.19 |
| | P3_130_090_12 | 90 | 12 | 128.1 | 77.7 | 104.4 | 103.19 | 10.7 |
| | P3_130_110_08 | 110 | 8 | 134.5 | 111.3 | 124.22 | 124.2 | 3.27 |
| | P3_130_110_10 | 110 | 10 | 132.2 | 116.6 | 124.25 | 124.03 | 2.21 |
| | P3_130_110_12 | 110 | 12 | 141.2 | 107.2 | 124.25 | 124.43 | 4.98 |
| | P3_130_130_08 | 130 | 8 | 155.4 | 127.3 | 144.18 | 144.43 | 4.99 |
| | P3_130_130_10 | 130 | 10 | 159.6 | 123.5 | 144.21 | 143.36 | 8.61 |
| | P3_130_130_12 | 130 | 12 | 178.6 | 118.2 | 144.11 | 143.16 | 12.06 |

## Annex D: Main statistical values – Tests 160 km/h

| *Pantograph* | Test name | Preload (N) | Span length (m) | Maximum force (N) | Minimum force (N) | Mean force (N) | Median (N) | Standard Deviation (N) |
|---|---|---|---|---|---|---|---|---|
| *1* | P1_160_070_08 | 70 | 8 | 104.5 | 77.4 | 91.55 | 91.13 | 5.11 |
| | P1_160_070_10 | 70 | 10 | 124.7 | 66.1 | 91.53 | 91.16 | 11.55 |
| | P1_160_070_12 | 70 | 12 | 133.6 | 52.5 | 91.42 | 89.58 | 18.14 |
| | P1_160_090_08 | 90 | 8 | 125.6 | 95.8 | 111.45 | 111.19 | 5.11 |
| | P1_160_090_10 | 90 | 10 | 143 | 83.4 | 111.41 | 111.3 | 10.87 |
| | P1_160_090_12 | 90 | 12 | 174 | 58.5 | 111.11 | 110.77 | 27.09 |
| | P1_160_110_08 | 110 | 8 | 147.1 | 114.2 | 131.36 | 131.21 | 5.27 |
| | P1_160_110_10 | 110 | 10 | 161.8 | 100.3 | 131.35 | 131.28 | 11.23 |
| | P1_160_110_12 | 110 | 12 | 216 | 64 | 130.81 | 129.21 | 37.23 |
| | P1_160_130_08 | 130 | 8 | 168.8 | 132.5 | 151.31 | 151.16 | 5.6 |
| | P1_160_130_10 | 130 | 10 | 180.5 | 116.6 | 151.24 | 150.85 | 12.52 |
| | P1_160_130_12 | 130 | 12 | 258.7 | 64.6 | 150.51 | 148.47 | 47.82 |
| *2* | P2_160_070_08 | 70 | 8 | 101.4 | 82.3 | 91.38 | 91.01 | 4.42 |
| | P2_160_070_10 | 70 | 10 | 108.7 | 78.5 | 91.32 | 90.37 | 5.86 |
| | P2_160_070_12 | 70 | 12 | 132.2 | 55.5 | 91.87 | 91.32 | 12.65 |
| | P2_160_090_08 | 90 | 8 | 122.8 | 99.6 | 111.8 | 112.28 | 4.24 |
| | P2_160_090_10 | 90 | 10 | 124.3 | 96.4 | 111.93 | 112.97 | 5.44 |
| | P2_160_090_12 | 90 | 12 | 168.3 | 62.7 | 111.74 | 109.09 | 18.73 |
| | P2_160_110_08 | 110 | 8 | 145.6 | 116.9 | 131.55 | 132.68 | 5.1 |
| | P2_160_110_10 | 110 | 10 | 144.9 | 111.7 | 131.78 | 132.5 | 6.32 |
| | P2_160_110_12 | 110 | 12 | 193.6 | 73.2 | 131.69 | 127.22 | 25.86 |
| | P2_160_130_08 | 130 | 8 | 164.7 | 136.8 | 151.41 | 151.4 | 5.45 |
| | P2_160_130_10 | 130 | 10 | 166.8 | 134 | 151.77 | 152.81 | 7.35 |
| | P2_160_130_12 | 130 | 12 | 218.3 | 83.2 | 151.65 | 146.58 | 33.16 |
| *3* | P3_160_070_08 | 70 | 8 | 114.5 | 71.6 | 91.64 | 91 | 7.46 |
| | P3_160_070_10 | 70 | 10 | 109.1 | 77.3 | 91.57 | 91.26 | 6.81 |
| | P3_160_070_12 | 70 | 12 | 154.7 | 31.3 | 91.57 | 89.12 | 26.94 |
| | P3_160_090_08 | 90 | 8 | 134.1 | 89.5 | 111.61 | 111.82 | 7.43 |
| | P3_160_090_10 | 90 | 10 | 131.7 | 92.5 | 111.59 | 112.26 | 7.2 |
| | P3_160_090_12 | 90 | 12 | 223.4 | 18.3 | 111.4 | 107.94 | 47.35 |
| | P3_160_110_08 | 110 | 8 | 154 | 107.2 | 131.58 | 132.85 | 7.63 |
| | P3_160_110_10 | 110 | 10 | 155.9 | 105.4 | 131.65 | 132.8 | 11.93 |
| | P3_160_110_12 | 110 | 12 | 292.6 | 1.8 | 131.23 | 126.88 | 68.46 |
| | P3_160_130_08 | 130 | 8 | 174.2 | 124.6 | 151.57 | 153.66 | 8.07 |
| | P3_160_130_10 | 130 | 10 | 183.7 | 118.3 | 151.68 | 153.02 | 17.78 |
| | P3_100_130_12 | 130 | 12 | 361.9 | 0 | 151.12 | 146.83 | 89.61 |

**Funding Sources**

This work was supported by the University of Málaga (PPIT.UMA.B1.2017/22).

**References**

[1] Patent n° FR2185838: “Ligne d’alimentation électrique rigide, notamment pour l’alimentation en courant de véhicules électriques sur rails (Rigid Overhead Current Conductor for ElectricRailways, in English)”, Delachaux, 1972.

[2] Chu, W.; Song, Y. Study on Dynamic Interaction of Railway Pantograph–Catenary Including Reattachment Momentum Impact. *Vibration* 2020, *3*, 18-33.

[3] S. P. Jung, Y. G. Kim, J. S. Paik, and T. W. Park,“Estimation of dynamic contact force between a pantograph and catenary using the finite element method,” Journal of Computational and Nonlinear Dynamics, vol. 7, no. 4, 2012. 2.2

[4] P. Nåvik, A. Rønnquist, and S. Stichel, “The use of dynamic response to evaluate and improve the optimization of existing soft railway catenary systems for higher speeds,” Proceedings of the Institution of Mechanical Engineers, Part F: Journal of Rail and Rapid Transit, vol. 230, no. 4, pp. 1388–1396, 2016.

[5] Yang Song, Pedro Antunes, Joao Pombo, Zhigang Liu, A methodology to study high-speed pantograph-catenary interaction with realistic contact wire irregularities, Mechanism and Machine Theory, Volume 152, 103940, 2020. ISSN 0094-114X, https://doi.org/10.1016/j.mechmachtheory.2020.103940.

[6] Vera C, Suarez B, Paulin J, Rodríguez P. Simulation model for the study of overhead rail current collector systems dynamics, focused on the design of a new conductor rail. Vehicle Syst Dynamics 2007;44(8):595–614. https://doi.org/10.1080/ 00423110500165499.

[7] Oya A, Shimizu M, Mandai T, Nishi K, Tago M. Application of overhead rigid conductor line to mountain tunnel of conventional lines. People’s Republic of China:Hong Kong; 2005. p. 170–4. 10.1109/ICIT.2005.1600630.

[8] Man M. Adoption of Overhead Rigid Conductor Rail System in MTR Extensions. Journal of International Council on. Electr Eng 2012;2(4):463–6. https://doi.org/ 10.5370/JICEE.2012.2.4.463.

[9] Montserrat Simarro, S. Postigo, Maria Prado-Novoa, A. Pérez-Blanca, Juan J. Castillo, Analysis of contact forces between the pantograph and the overhead conductor rail using a validated finite element model, Engineering Structures, Volume 225, 2020, 111265, ISSN 0141-0296, https://doi.org/10.1016/j.engstruct.2020.111265.

[10] Railway Gazette. Rigid catenary speed record [EB/OL]. http://www.railwaygazette.com/news/infrastructure/single-view/view/rigid-catenary-speed-record.html. Accessed 07 October 2020

[11] EN 50367. Railway applications - Current collection systems - Technical criteria for the interaction between pantograph and overhead line (to achieve free access). 2012.

[12] J. Pombo, J. Ambrósio, M. Pereira, "Influence of Pantograph Components on the Contact Quality of the Overhead System for High Speed Trains", in B.H.V. Topping, J.M. Adam, F.J. Pallarés, R. Bru, M.L. Romero, (Editors), "Proceedings of the Tenth International Conference on Computational Structures Technology", Civil-Comp Press, Stirlingshire, UK, Paper 1, 2010. doi:10.4203/ccp.93.1

[13] Bucca G, Carnevale M, Collina A, Facchinetti A, Drugge L, Jönsson P-A, Stichel S. Adoption of different pantographs' preloads to improve multiple collection and speed up existing lines. Veh Syst Dyn. 2012;50(suppl 1):403–418.

[14] Takemura T, Fujii Y, Shimizu M. Characteristics of overhead rigid conductor line having T-type cross section. Proceedings of the IEEE International Conference on Developments in Mass Transit Systems, London, UK. 1998. p. 173–7. 10.1049/cp:19980115.

[15] Chen L., Liu Z., Zhang J., Hu Z. Influence of Key Parameters on High Speed Overhead Conductor Rail and Pantograph System. In: Klomp M., Bruzelius F., Nielsen J., Hillemyr A. (eds) Advances in Dynamics of Vehicles on Roads and Tracks. IAVSD 2019. Lecture Notes in Mechanical Engineering. Springer, Cham. https://doi.org/10.1007/978-3-030-38077-9_25.

[16] Juan de Dios Sanz, Álvaro Calvo, David Barbado, Analysis of the capability of non-specific simulation software for studying the dynamic interaction between pantograph and rigid overhead conductor rail, Transportation Research Procedia, Volume 33, 2018, Pages 187-194, ISSN 2352-1465, https://doi.org/10.1016/j.trpro.2018.10.091.

[17] Bautista A, Montesinos J, Pintado P. Dynamic interaction between pantograph and rigid overhead lines using a coupled FEM - multibody procedure. Mechanism and Machine Theory 2016; 97, 100-111. https://doi.org/10.1016/j.mechmachtheory.2015.10.009.

[18] Calleja V, Fernández RA, Barreiro J, Calvo A. Development and testing of a tuned mass damper for overhead contact rail systems. Dyna. 2017. 92:6, 680-687. https://dx.doi.org/10.6036/8498

[19] X.K. Wei, H.F. Meng, J.H. He, L.M. Jia, Z.G. Li, Wear analysis and prediction of rigid catenary contact wire and pantograph strip for railway system, Wear, Volumes 442–443, 203118, 2020, ISSN 0043-1648, https://doi.org/10.1016/j.wear.2019.203118.

[20] Guiming Mei, Tribological performance of rigid overhead lines against pantograph sliders under DC passage, Tribology International, Volume 151, 2020, 106538, ISSN 0301-679X, https://doi.org/10.1016/j.triboint.2020.106538...

[21] Carnevale M, Collina A, Zuin A. A rolling stock-based system for catenary condition monitoring: Validation through numerical simulations on a rigid catenary. Proceedings of the Mini Conference on Vehicle System Dynamics, Identification and Anomalies, 2019-November, pp. 209-217.

[22] M. Tur, E. García, L. Baeza, and F. J. Fuenmayor, "A 3D absolute nodal coordinate finite element model to compute the initial configuration of a railway catenary," *Eng. Struct.*, vol. 71, pp. 234– 243, 2014.

[23] Ning Zhou, Weihua Zhang, Investigation on dynamic performance and parameter optimization design of pantograph and catenary system, Finite Elements in Analysis and Design, Volume 47, Issue 3, 2011, Pages 288-295, ISSN 0168-874X, https://doi.org/10.1016/j.finel.2010.10.008.

[24] S. P. Jung, Y. G. Kim, J. S. Paik, and T. W. Park,"Estimation of dynamic contact force between a pantograph and catenary using the finite element method," Journal of Computational and Nonlinear Dynamics, vol. 7, no. 4, 2012. 2.2.

[25] Simarro, S. Postigo, Juan A. Cabrera, Juan J. Castillo, A procedure for validating rigid catenary models using evolutionary techniques, Computers & Structures, Volume 228, 2020, 106145, ISSN 0045-7949, https://doi.org/10.1016/j.compstruc.2019.106145.

[26] Pombo J, Ambrósio J, Pereira M, Rauter F, Collina A, Facchinetti A. Influence of the aerodynamic forces on the pantograph–catenary system for high-speed trains. Veh Syst Dyn 2009;47(11):1327–47. https://doi.org/10.1080/00423110802613402.

[27] Seo Jong-Hwi, Sugiyama Hiroyuki, Shabana Ahmed A. Three-Dimensional Large Deformation Analysis of the Multibody Pantograph/Catenary Systems. Nonlinear Dyn 2005;42(2):199–215. https://doi.org/10.1007/s11071-005-2789-9.

[28] Collina A, Bruni B. Numerical simulation of pantograph overhead equipment interaction. Veh Syst Dyn 2002;38(4):261–91. https://doi.org/10.1076/vesd.38.4. 261.8286.

[29] Collina A, lo Conte A, Marco C. Effect of collector deformable modes in pantograph– catenary dynamic interaction. Proceedings of The Institution of Mechanical Engineers Part F-journal of Rail and Rapid Transit 14 January 2009, 223. doi:10. 1243/09544097JRRT212.

[30] Zhou N, Wei-hua Zhang W, Li R. Dynamic performance of a pantograph-catenary system with the consideration of the appearance characteristics of contact surfaces. J Zhejiang Univ-Sci A (Appl Phys Eng) 2011;12(12):913–20. https://doi.org/10.1631/jzus.A11GT015.

[31] Ambrósio Jorge, Pombo João, Pereira Manuel. Optimization of high-speed railway pantographs for improving pantograph-catenary contact. Theor Appl Mech Lett 2013;3:1. https://doi.org/10.1063/2.1301306.

[32] Yong Hyeon Cho, Kiwon Lee, Young Park, Bubyoung Kang, Ki-nam Kim, Influence of contact wire pre-sag on the dynamics of pantograph–railway catenary, International Journal of Mechanical Sciences, Volume 52, Issue 11, 2010, Pages 1471-1490, ISSN 0020-7403, https://doi.org/10.1016/j.ijmecsci.2010.04.002.

[33] Stefano Bruni, Jorge Ambrosio, Alberto Carnicero, Yong Hyeon Cho, Lars Finner, Mitsuru Ikeda, Sam Young Kwon, Jean-Pierre Massat, Sebastian Stichel, Manuel Tur, Weihua Zhang. The results of the pantograph–catenary interaction benchmark, Vehicle System Dynamics. 2015. 53:3, 412-435, doi: 10.1080/00423114.2014. 953183.

[34] Yan-long Shen, Ying Wang, Xiao-qiang Chen, Li Cao, Ming-xin Tian. Wavelength Component Analysis of the Pantograph-catenary Contact Force Based on EEMDSPWVD. 2018. International Conference on Computational, Modeling, Simulation and Mathematical Statistics. doi: 10.12783/dtcse/cmsms2018/25207.

[35] EN 50318, Validation of simulation of the dynamic interaction between pantographs and overhead contact Line, CENELEC, 2002.

[36] Carnevale M, Facchinetti A, Maggiori L, et al. Computational fluid dynamics as a means of assessing the influence of aerodynamic forces on the mean contact force acting on a pantograph. Proc Inst Mech Eng Part F J Rail Rapid Transit. 2016;230:1698–1713. doi:10.1177/ 0954409715606748

[37] Petter Nåvik, Anders Rønnquist & Sebastian Stichel (2017). Variation in predicting pantograph–catenary interaction contact forces, numerical simulations and field measurements, Vehicle System Dynamics, 55:9, 1265-1282, DOI: 10.1080/00423114.2017.1308523

[38] J. Pombo, J. Ambrósio. Environmental and track perturbations on multiple pantograph interaction with catenaries in high-speed trains. Computers and Structures, 2013. Vol 124. pp:88-101. http://dx.doi.org/10.1016/j.compstruc.2013.01.015

[39] Carnicero, J. R. Jimenez-Octavio, C. Sanchez-Rebollo, A. Ramos and M. Such, Influence of track irregularities in the catenary-pantograph dynamic interaction, J. Comput. Nonlinear Dyn., vol. 7, no. 4, Oct. 2012.

[40] Y. Song, Z. Liu, A. Rønnquist, P. Nåvik, and Z. Liu, Contact wire irregularity stochastics and effect on high-speed railway pantograph-catenary interactions, IEEE Trans. Instrum. Meas., vol. 69, no. 10, pp. 8196-8206, Oct. 2020, doi: 10.1109/TIM.2020.2987457.

[41] Chao Huang, Anbin Wang , Xiaohan Gu, Xiaogang Gao, Yu He, Lang Liu, and Feng Gao. High-frequency vibration analysis and optimization of irregular wear of pantograph carbon strips. shock and vibration. Volume 2020, Article ID 8850079, 15 pages. https://doi.org/10.1155/2020/8850079

[42] Hongrui Wang, Zhigang Liu, Alfredo Núñez and Rolf Dollevoet. Entropy-based local irregularity detection for high-speed railway catenaries with frequent inspections IEEE Transactions on Instrumentation and Measurement, VOL. 68, NO. 10, October 2019.

[43] Ambrosio J, Pombo J, Pereira M, Antunes P, Mosca A. Recent Developments in Pantograph-Catenary Interaction Modelling and Analysis. Int J Railway Technol. 2012;1(1):249–78. https://doi.org/10.4203/ijrt.1.1.12.